Turun yliopisto
University of Turku

Ring Dark Solitons in Toroidal Bose-Einstein Condensates

Lauri A. Toikka

ACADEMIC DISSERTATION

To be presented, with the permission of the Faculty of Mathematics and Natural Sciences at the University of Turku, for public examination in the Tauno Nurmela auditorium on the 18th of June, 2014, at 12 o'clock.

TURUN YLIOPISTON JULKAISUJA - ANNALES UNIVERSITATIS TURKUENSIS
SARJA - SER. A I OSA - TOM. 489 | ASTRONOMICA - CHEMICA - PHYSICA - MATHEMATICA
Turku 2014

University of Turku

Faculty of Mathematics and Natural Sciences
Department of Physics and Astronomy
Turku Centre for Quantum Physics
Laboratory of Quantum Optics

Supervised by

Kalle-Antti Suominen
Professor of Physics
Department of Physics and Astronomy
University of Turku, Finland

Reviewed by

Thomas Busch
Associate Professor
Quantum Systems Unit
OIST, Japan

Tapio Simula
Monash Fellow
School of Physics
Monash University, Australia

Opponent

Natalia G Berloff
Professor of Applied Mathematics
Department of Applied Mathematics and Theoretical Physics
University of Cambridge (Jesus College), UK

Front cover picture by Lea Toikka. Revival of a ring dark soliton in terms of the density and phase dynamics. See Sec. 5.2.

The originality of this Thesis has been checked in accordance with the University of Turku quality assurance system using the Turnitin OriginalityCheck service.

ISBN 978-951-29-5738-5 (PRINT)
ISBN 978-951-29-5739-2 (PDF)
ISSN 0082-7002
Painosalama Oy - Turku, Finland 2014

Acknowledgements

I am indebted to many people who have had an effect towards the completion of this Thesis. It forms a portfolio for the work conducted at the Turku Centre for Quantum Physics in 2010 – 2013 under the skillful guidance and supervision of professor Kalle-Antti Suominen.

Despite his vice-rectorship and other commitments, Kalle-Antti has always had the time to discuss results and ideas (both silly and useful) with profound insight, and I would like to extend my best thanks. These discussions have drastically reduced the time spent floundering, and I have learned a considerable amount of conducting scientific work from you. Also, the lessons taught by Dr. Raphael Blumenfeld during my undergraduate times at Cambridge have turned out to be helpful in many ways.

During the years, I have had the privilege of attending various summer schools (the Graduate School of Modern Optics and Photonics Summer School 2012 in Joensuu, ICAP 2012 in Paris, Les Houches 2012, IQSD 2013 in Espoo, the Young Atom Opticians Conference 2013 in Birmingham, and the Victorian Summer School in Ultracold Physics 2014 in Melbourne). These events have been very valuable.

In the final year, sharing the office with Jaakko Lehto has enabled easy access to his well-thumbed copy of Abramowitz and Stegun. I have been careful with it. Down the corridor, Vladimir S. Ivanov has enlightened the atmosphere by discussions. I would also like to thank Dr. Aidan Arnold (Strathclyde) and Dr. Tapio Simula (Monash) for hospitality and making it possible for me to give talks, and Drs. Thomas Busch and Tapio Simula for the time and effort to review this Thesis. In addition, I am thankful to professor Natalia Berloff for serving as the opponent in the formal defense. Financial support by Suomen Kulttuurirahasto, Turun suomalainen yliopistoseura, Jenny ja Antti Wihurin rahasto, and Academy of Finland (grant 133682) is acknowledged.

Outside of physics, I have enjoyed swimming in Aurajoen Uinti. Milliksen hurjat has provided a friendly swimming group for the Friday practices.

Last, I would like to express my gratitude to Wojtek, Bern, Dennis, and other friends and family for all the support. David, *Ti voglio bene, sei un amico! :)*

Turku, May 2014
Lauri A. Toikka

Contents

Abstract

In this Thesis, we study various aspects of ring dark solitons (RDSs) in quasi-two-dimensional toroidally trapped Bose-Einstein condensates, focussing on atomic realisations thereof.

Unlike the well-known planar dark solitons, exact analytic expressions for RDSs are not known. We address this problem by presenting exact localised soliton-like solutions to the radial Gross-Pitaevskii equation. To date, RDSs have not been experimentally observed in cold atomic gases, either. To this end, we propose two protocols for their creation in experiments.

It is also currently well known that in dimensions higher than one, (ring) dark solitons are susceptible, in general, to an irreversible decay into vortex-antivortex pairs through the snake instability. We show that the snake instability is caused by an unbalanced quantum pressure across the soliton's notch, linking the instability to the Bogoliubov-de Gennes spectrum. In particular, if the angular symmetry is maintained (or the toroidal trapping is restrictive enough), we show that the RDS is stable (long-lived with a lifetime of order seconds) in two dimensions. Furthermore, when the decay does take place, we show that the snake instability can in fact be reversible, and predict a previously unknown revival phenomenon for the original (many-)RDS system: the soliton structure is recovered and all the point-phase singularities (i.e. vortices) disappear. Eventually, however, the decay leads to an example of quantum turbulence; a quantum example of the laminar-to-turbulent type of transition.

Finnish Abstract

Tässä työssä käsitellään pimeitä rengassolitoneja litteissä kaksiulotteisissa atomisissa Bosen-Einsteinin kondensaateissa. Toisin kuin suorat pimeät solitonit, pimeälle rengassolitonille ei ole tiedossa analyyttista kaavaa. Väitöskirjan ensimmäisessä julkaisussa esitellään muun muassa uusia eksakteja rengassolitonin kaltaisia ratkaisuja Grossin-Pitaevskiin yhtälölle. Väitöskirjassa kehitetään ja esitellään myös kaksi kokeellista menetelmää pimeiden rengassolitonien luomiseen laboratoriossa. Pimeiden rengassolitonien hajoamista ja sitä seuraavaa vorteksi-antivorteksiparien fysiikkaa tutkitaan väitöskirjan loppupuolella. Osoitetaan, että pimeän solitonin hajoaminen ei olekaan peruuttamatonta kuten aiemmin on luultu, vaan se on mahdollista, mikäli atomiloukun muoto valitaan sopivasti.

List of Publications

This Thesis consists of an introductory review, and the following five articles:

I *Exact soliton-like solutions of the radial Gross-Pitaevskii equation*
L. A. Toikka, J. Hietarinta, and K.-A. Suominen
J. Phys. A: Math. Gen. **45**, 485203 (2012)

II *Snake instability of ring dark solitons in toroidally trapped Bose-Einstein condensates*
L. A. Toikka and K.-A. Suominen
Phys. Rev. A **87**, 043601 (2013)

III *Creation and revival of ring dark solitons in an annular Bose-Einstein condensate*
L. A. Toikka, O. Kärki, and K.-A. Suominen
J. Phys. B: At. Mol. Opt. Phys. **47**, 021002 (2014)

IV *Self-interference of a toroidal Bose-Einstein condensate*
L. A. Toikka
New J. Phys. **16**, 043011 (2014)

V *Reversible decay of ring dark solitons*
L. A. Toikka and K.-A. Suominen
J. Phys. B: At. Mol. Opt. Phys. **47**, 085301 (2014)

Other Articles

- *Response of mechanically strained nanomaterials to irradiation: Insight from atomistic simulations*
  E. Holmström, L. A. Toikka, A. V. Krasheninnikov, and K. Nordlund
  Phys. Rev. B **82**, 045420 (2010)

- *From Kepler to Lord Kelvin: A modern approach to the particle packing problem*
  L. A. Toikka and R. Blumenfeld
  Manuscript in preparation

Chapter 1

Introduction

"Be curious."
Stephen Hawking (2013)

Here on the Earth, our brains have evolved to deal with and understand the everyday states of matter at the everyday temperatures and pressures: solid, liquid, gas, and plasma[1]. The physics of these states has been studied for centuries, and a myriad of important results is already known. In fact, in the 21st century, we are in a position to term this physics *classical*. Due to the lack of equally immediate correspondence to the natural environment occurring on the surface of this planet, not all of the possible states of matter have been so thoroughly studied. The reach of these more exotic phases can lie behind barriers that demand significant experimental effort, and they can occur in the regime of *quantum mechanics*: the physics of the very small and very cold, which is often completely unintuitive to us.

For many applications, it would be convenient if the quantum world could be studied and subsequently harnessed on a larger scale. Full control of quantum phenomena on truly macroscopic scales of space and time would in fact be the physics headlines of the century. Unfortunately, quantum systems are extremely fragile, and as the properties of the systems approach everyday values, interaction with the environment quickly leads to decoherence and the quantum-to-classical transition, destroying the quantum features in the

[1]Plasma is encountered in lightnings, for example. There are approximately 100 occurrences worldwide every second [1], but fortunately, assuming a Poissonian process and using the Finnish averages, we can calculate that the chance of being struck by one in a lifetime is only $\sim 1/8224$.

process [2]. The state of ultra-cold matter called a *Bose-Einstein condensate* (BEC) is a modern example of the best of both worlds, which are nowadays prepared by many groups around the world as a matter of routine. BECs are quintessentially quantum mechanical objects with long-range phase coherence, but with sizes on the order of a few µm and lifetimes spanning seconds. Not surprisingly, they have attracted an explosion of research interest in the past two decades, with many milestones along the way being recognised by the Nobel Foundation.

Following the major advances in laser and evaporative cooling of alkali atoms [3–5], the first definitive experimental realisations of Bose-Einstein condensation were achieved in 1995 using vapours of the bosonic alkali gases ^{87}Rb and ^{23}Na [6, 7]. The condensates are dilute (the mean number density $n_{\mathrm{BEC}} \sim 10^{12}\,\mathrm{cm}^{-3}$ to $10^{15}\,\mathrm{cm}^{-3}$ [8], cf. $n_{\mathrm{air}} \sim 10^{19}\,\mathrm{cm}^{-3}$ and $n_{\mathrm{water}} \sim 10^{22}\,\mathrm{cm}^{-3}$), which results in an ultra-low critical temperature in the nanokelvins[2] for the phase transition into the BEC state, but typical length scales are on the order of 10 µm to 100 µm.

Originally, the concept of BEC existed as a theoretical notion discovered by Bose and Einstein in the 1920s. They predicted a phase transition of non-interacting bosons below a certain critical temperature [10, 11], but the concept has since been linked with exciting phenomena such as superfluidity in liquid ^{4}He [12, 13] in the interacting regime [14, 15]. The link has not been as straightforward to establish experimentally, though. Neutron scattering experiments [16, 17] and numerical simulations [18] have shown that the condensate fraction is only about 7 % to 8 %, and getting smaller as $T \to T_\lambda$ from below, where $T_\lambda = 2.17\,\mathrm{K}$ (ambient pressure) is the temperature corresponding to the λ-line of the He-I (normal phase) to He-II (superfluid) transition. In fact, the relatively low condensate occupancy in superfluid helium is caused by the strong inter-particle interactions, which are caused by the helium existing as a liquid at the lowest temperatures under any relevant pressure[3].

In general, however, BEC is neither necessary nor sufficient for superfluidity[4]. As discussed above, at $T = 0$ in ^{4}He, the whole liquid can be superfluid despite only $\sim 10\,\%$ of the atoms being in the condensed fraction.

[2] Quite possibly the coldest temperatures in the whole Universe! The cosmic microwave background radiation has a thermal black body spectrum corresponding to a temperature of $2.72548 \pm 0.00057\,\mathrm{K}$ [9].

[3] The small atomic mass of helium makes the quantum zero-point energy large enough to inhibit crystallisation; at $T < T_\lambda$, liquid ^{4}He needs a pressure in excess of 2.5 MPa ($\sim 25\,\mathrm{atm}$) to solidify [8].

[4] Like quantum turbulence, superfluidity encompasses a range of phenomena which normally occur in conjunction [19].

Furthermore, it turns out that the phenomenon of BEC is not possible in an infinite two-dimensional system unless the temperature is zero [20, 21]. This follows from quantum phase fluctuations - the phase correlation length has a non-zero limit at infinity (see Sec. 2.1) making BEC possible only at $T = 0$. At non-zero but small temperatures $T > 0$, the physics is described by the Berezinskii-Kosterlitz-Thouless (BKT) phase [22, 23], with correlation functions decaying algebraically to zero at large distance making the true BEC phase impossible, but still with stronger coherence than a thermal gas with exponential decay. The finite temperature causes the excitation and proliferation of vortices, and in the BKT phase there is superfluid order through the formation of vortex-antivortex pairs. Nevertheless, BECs are usually superfluid.

Because of the lower density, in a gaseous cloud (of neutral particles), the particles are in general much more weakly interacting with each other than in the liquid phase, and correspondingly, one can expect the condensate fractions of Bose alkali gases to be conveniently higher. However, at the ultra-cold temperatures (on the order of nano- to microkelvins) required for quantum degeneracy, one might (quite reasonably!) expect the thermodynamical equilibrium to entail a crystalline solid. Still, the crystallisation can in fact be avoided [5]. The key is the extreme diluteness: $n_{\mathrm{BEC}}/n_{\mathrm{air}} \sim 10^{-6}$. As the formation of a dimer in practice needs a three-body collision[5], the rate per atom of which happening is $\propto n_{\mathrm{BEC}}^2$, the time scales associated with the formation of molecules ($\propto n_{\mathrm{BEC}}^{-2}$) and eventually solids (or small clusters) are so long that a quasi-stable gaseous phase can be maintained. Subsequently, BEC can be obtained and experimented on.

As a result of the diluteness[6] of the alkali atom BECs, a mean-field description is exceedingly accurate, and the condensate fraction is close to the total number of particles. The condensates are also large [$\sim \mathcal{O}(\mu\mathrm{m})$] and can contain between $\mathcal{O}(10^2)$ to $\mathcal{O}(10^9)$ atoms. They can be confined with magnetic traps or optically with laser light, but for our purposes the external trap

[5] Two-body collisions in free space are surpassingly improbable to produce dimers because of the stringent boundary conditions set by conservation laws of various quantities. The presence of a third particle allows for many more ways to distribute the energy, angular momentum [19], etc. The number density is then limited by the three-body losses.

[6] In the sense that the s-wave scattering length a_{s} (see Sec. 2.2) is much smaller than the inter-particle spacing; i.e. the gas parameter $\zeta \equiv \sqrt{n_{\mathrm{BEC}} a_{\mathrm{s}}^3} \ll 1$. Typically $a_{\mathrm{s}} \sim \mathcal{O}(\mathrm{nm})$ for the dilute alkalis. Then ζ is small and provides the expansion parameter in the Bogoliubov theory [24]. The mean-field Gross-Pitaevskii equation (GPE) (see Sec. 2.2) is then given by the lowest order, when terms of relative order ζ can be neglected (but, see Ref. [25] for an elaborate discussion of subtleties). Correspondingly, the GPE is not a good model for superfluid ^{4}He, but it is an excellent model for ultra-cold dilute Bose alkali gases (at $T \approx 0$).

is given by a potential term without explicit reference to the physical origin[7]. Typically, optical traps are used to avoid the strength of the inter-particle interactions from varying spatially near to a Feshbach resonance [27], while magnetic traps can be used in evaporative cooling, a widely used final stage in achieving condensation. In addition, we can apply a tight harmonic trap in the z-direction so that the BEC is reduced to the corresponding ground state, and projected as a quasi-two-dimensional condensate in the xy-plane [28], taking the shape of a pancake. On toroidal geometry, the central region is forbidden, and indeed ring traps [29–37] have attracted significant interest. A toroidal quasi-two-dimensional BEC is the physical system considered in this Thesis.

The equation of motion for the BEC in the mean-field approximation at $T \approx 0$ is the celebrated *Gross-Pitaevskii equation* (GPE) [38, 39], or variably, depending on context, called the *nonlinear Schrödinger equation* (NLS). It is a nonlinear partial differential equation for the macroscopic wave function of the BEC, where the nonlinearity arises from the mean-field interaction.

The nonlinearity of the GPE allows for interesting solutions such as bright and dark solitons [8, 40–42], which remarkably propagate without dispersion [43] and scatter elastically. The importance of solitons is their ubiquitousness in physics and also biology [44] (note that the NLS is only one example of an integrable soliton equation). Mathematically, there exists rich structure in the theory of solitons [45–48]. In BECs and superfluid Fermi gases [49–52], matter-wave solitons correspond to shape-maintaining dips or humps in the atomic density. Perhaps more usefully from a technological point of view, soliton light pulses sent through optical fibers propagate without changing shape and can therefore be sent in rapid succession[8]. In gauge theories of high energy physics [53–55], it has been proposed that (elementary) particles be thought of as solitons as they scatter elastically, are localised and have a well-defined finite energy; they retain their identity (cf. the form-stability above).

Dark solitons have been observed experimentally [56, 57], but strictly speaking the stability holds only in one-dimensional systems. In higher dimensions, in general, they collapse into vortex-antivortex pairs in 2D (or vortex rings in 3D) through the snake instability [58, 59], even though dark solitons retain many of their solitonic properties in nearly-integrable systems, for example, in the presence of an external trap [60]. The stability and dy-

[7] For a review of various experimental trapping techniques, we refer the reader to e.g. Refs. [8, 26].

[8] In the nonlinear optics setting, the NLS describes the evolution of the complex amplitude of the electric field.

namics of dark solitons has been discussed theoretically [61–64], in particular, complex frequencies in the Bogoliubov-de Gennes excitation spectrum have been demonstrated to drive the instability [65].

Cylindrically symmetric systems, bringing forward the concepts of ring bright [66] and dark [67–70] solitons (RDSs), offer an example of a two-dimensional system, where the dynamics can be reduced to a one-dimensional equation, and thereby making the question of stability relevant. It has been shown using perturbation theory that a small amplitude NLS RDS is described by the cylindrical Korteweg-de Vries equation [67]. However, as far as exactness is concerned, the obtained results are valid only for an infinitesimally shallow RDS, i.e. a soliton that is indistinguishable from the background! In particular, in this Thesis, we study various aspects of ring dark solitons in quasi-two-dimensional atomic BECs confined in a ring trap.

In addition to being a controlled testbed for many-body physics [71, 72] and all the various phenomena observed so far (for a review, see e.g. Refs. [8, 19]), the field of ultra-cold quantum liquids is growing at a fast pace. New fields such as artificial gauge potentials [73] (simulated magnetism) are emerging. Ultra-cold quantum liquids have been proposed to serve as simulators for many phenomena in high energy physics and cosmology as well - indeed, even for the whole Universe in and of itself [74]!

This Thesis is organised as follows:

Chapter 2: We present the relevant theoretical background to the topics discussed in the later chapters.

Chapter 3: We present an introduction to Publication I, discussing how to find solutions to the radial Gross-Pitaevskii equation. Some new previously unpublished solutions are presented.

Chapter 4: We present two protocols for the experimental creation of ring dark solitons, which are considered in Publications III and IV. We discuss how the self-interference appearing in the protocols can be seen in the Wigner function, and with the method of images.

Chapter 5: We present an introduction to the snake instability (Publication II) and revival dynamics (Publication V) of ring dark solitons.

Chapter 6: We summarise the research in Publications I-V, and present an outlook for future directions.

Chapter 2

Interacting Atomic Bose-Einstein Condensates

Bose-Einstein condensation can be viewed as a classical thermal phase transition: below a critical temperature T_c, the bosons making up the system condense into a single one-body state described by the condensate wave function ψ, which plays the role of the order parameter of the transition. On the other hand, we can quench the effect of the temperature by focussing on the case $T = 0$ and taking the chemical potential μ as the control parameter of the transition. In this case, there is a (quantum) phase transition into the BEC state as μ becomes zero (from below).

In loose terms, the chemical potential μ is to occupation numbers what the temperature T is to heat distributions. To be more specific, at constant pressure, the Gibbs-Duhem relation

$$N \, \mathrm{d}\mu = -S \, \mathrm{d}T + V \, \mathrm{d}p, \tag{2.1}$$

where p, V, S, and N are the pressure, volume, entropy and number of particles respectively, shows that if the entropy S decreases when particles are being removed, then μ will increase as the temperature decreases. The physical relevance of this notion in a system of N (non-interacting) bosons can be understood from the Bose-Einstein distribution for the average number of bosons in the one-body state i with energy ϵ_i, n_i, at temperature T:

$$n_i(\mu, T) = \frac{1}{\exp\left(\frac{\epsilon_i - \mu}{k_\mathrm{B} T}\right) - 1}, \tag{2.2}$$

where k_B is the Boltzmann constant, and the chemical potential μ is locked by the total number of particles N:

$$N = N_0 + \sum_{i>0} n_i(\mu, T), \tag{2.3}$$

where N_0 is the number of particles in the ground state. As the temperature T is reduced whilst keeping N constant, Eqs. (2.2) and (2.3) require that μ increases.

Note that Eq. (2.2) only makes sense if $\mu \leq \epsilon_0$. If we assume $\epsilon_0 = 0$ and $\epsilon_i \geq 0$, then $\mu \leq 0$. In particular, at some critical temperature T_c, the chemical potential reaches zero, and there are as many particles as possible in the excited states $i > 0$. For $T < T_\mathrm{c}$, the chemical potential must remain constant at zero, and as a result, a macroscopic number *Bose-Einstein condenses* (in the simplest possible non-fragmented case, see Sec. 2.1) into the ground state with energy ϵ_0. Otherwise, there would be unphysically many particles in the excited states, and the system could lose energy by decaying to lower levels. In this case, the positive chemical potential $\mu > 0$ would be analogous to a negative (absolute) temperature $T < 0$, which is hotter than infinitely hot. Any other configuration would have a positive μ, and the availability of the BEC state with the lower $\mu = 0$ drives the phase transition[1].

It turns out [8] that for a uniform gas (number density n) of non-interacting bosons in a box in three dimensions, the critical temperature T_c is determined by

$$T_\mathrm{c} = \frac{2\pi\hbar^2}{m k_\mathrm{B}} \left(\frac{n}{\zeta\left(\frac{3}{2}\right)} \right)^{\frac{2}{3}}, \tag{2.4}$$

where $\hbar$ is the reduced Planck constant, ζ is the Riemann zeta-function, and m is the mass of the bosons. For $T < T_\mathrm{c}$, there exists non-zero macroscopic occupation of the single-particle ground state. The number of particles in the condensate N_0, is given by

$$N_0 = N \left[1 - \left(\frac{T}{T_\mathrm{c}} \right)^{\frac{3}{2}} \right], \tag{2.5}$$

where N is the total number of particles in the gas [and satisfies $N = N_0 + N_\mathrm{e}$, where N_e is the number of particles in excited states, see Eq. (2.3)]. These results assume that $N \gg 1$.

While the finite-T phase transition can be understood in terms of classical thermodynamics alone, we emphasise that the BEC phase is quantum mechanical in nature. Quantum statistics, and in particular, the fundamental indistinguishability[2] of the bosons, matter. The relevant distribution is

[1] E.g. cf. the phase transition between liquid water and water vapour. When $\mu_\mathrm{vapour} > \mu_\mathrm{liquid}$, the water condenses. Note from Eq. (2.1) that changes in μ depend in general on pressure and temperature - on top of Mount Everest (8848 m), the lower pressure causes water to boil at 71 °C; the boiling point decreases by 1 °C every ~ 300 m of elevation.

[2] In that they cannot be tagged or kept track of, unlike classical particles by e.g. their position.

Eq. (2.2) instead of the classical Maxwell-Boltzmann distribution, which is its high-temperature and low-density limit. The importance of particle indistinguishability can be seen by considering the thermal de Broglie wavelength $\lambda_{\mathrm{T}} \sim h/p$, where p is the mean momentum per particle and h the Planck constant, of an ideal gas of atoms in three dimensions. It is determined by the equilibrium temperature T and mass m of the particles through $\lambda_{\mathrm{T}} \sim h/\sqrt{mk_{\mathrm{B}}T}$. If the de Broglie wavelengths of the atoms were to overlap, it would be fundamentally impossible to tell to which atom an observed non-zero density at some point in space belongs, as they are indistinguishable. This overlap happens at low temperatures, when $\lambda_{\mathrm{T}} \gtrsim \lambda$, where $\lambda \sim n^{-1/3}$ is the mean inter-particle spacing and n the mean number density. In this regime, the gas is degenerate and the phase-space density $n\lambda_{\mathrm{T}}^3 \sim \mathcal{O}(1)$; the quantum statistics (through the indistinguishability) of the particles become important. For example, the phase-space density corresponding to Eq. (2.4) is $n\lambda_{\mathrm{T}}^3 = \zeta\left(\frac{3}{2}\right) \approx 2.612$.

We have encountered the simplest possible example of BEC in terms of non-interacting bosons in free space. While it is remarkable that such an example exists, it is not a very satisfying explanation for the phenomenon of BEC. For example, the Bose-Einstein distribution (2.2) has a singularity at $\mu = \epsilon_0$. This would not be a major problem for massless photons[3] with zero energy and therefore infinite wavelength, but for massive Bose alkali atoms we had to separate the occupancy of the lowest state in Eq. (2.3). Also, the example tells nothing about the effect of inter-particle interactions.

2.1 Definitions of BEC

To address the occurrence of BEC in an interacting system of spinless bosons more precisely, we consider the properties of the single-particle (or reduced) density operator $\hat{\rho}_1 = \mathrm{Tr}_{2\ldots N}(\hat{\rho})$, where $\hat{\rho}$ is the density operator and the trace is over all the other particles except for particle number 1 (without loss of generality as all the bosons are indistinguishable). For a more thorough discussion of the various definitions considered here, see Ref. [19].

The first definition we consider is originally given in Ref. [15]. It follows from the hermiticity of the density operator ($\hat{\rho}^\dagger = \hat{\rho}$) that $\hat{\rho}_1$ is Hermitian, and therefore can be diagonalised with the eigenstates forming a complete normalisable orthogonal set: we write $\hat{\rho}_1(t) = \sum_i n_i(t)\,|\chi_i(t)\rangle\,\langle\chi_i(t)|$. In the

[3] The condensation of which has been observed [75], although the nature of a photon inside a medium is somewhat subtle. If the photon interacts with the medium, at some point it becomes meaningful to talk about polariton quasi-particles instead.

position representation,

$$\rho_1(\mathbf{r},\mathbf{r}';t) = \langle\hat{\psi}^\dagger(\mathbf{r},t)\hat{\psi}(\mathbf{r}',t)\rangle = \sum_i n_i(t)\chi_i^*(\mathbf{r},t)\chi_i(\mathbf{r}',t), \tag{2.6}$$

where $\hat{\psi}(\mathbf{r},t)$ is the position representation of the bosonic annihilation operator. It satisfies $[\hat{\psi}(\mathbf{r},t),\hat{\psi}(\mathbf{r}',t)] = [\hat{\psi}^\dagger(\mathbf{r},t),\hat{\psi}^\dagger(\mathbf{r}',t)] = 0$ and $[\hat{\psi}^\dagger(\mathbf{r},t),\hat{\psi}(\mathbf{r}',t)] = \delta(\mathbf{r}-\mathbf{r}')\,\forall\,\mathbf{r},\mathbf{r}'$, the bosonic commutation algebra. In effect, it is an operator-valued field ($\mathbf{r}$ is continuous), a quantum field, which annihilates a boson at the location $\mathbf{r}$ at time t.

Definition 1. *Exactly one of the eigenvalues $\{n_i\}$ is of order N, and all the others are of order unity $\leftrightarrow$ Simple (non-fragmented) BEC.*

When $\mathbf{r} = \mathbf{r}'$, the reduced density matrix equals the particle density n: $\rho_1(\mathbf{r},\mathbf{r};t) = n(\mathbf{r},t)$. We can see that according to the above definition, the case of the non-interacting gas considered in Sec. 2 is an example of simple BEC.

Note that Definition 1 applies to interacting and non-interacting cases alike because $\hat{\rho}_1$ is defined in either case. The average of Eq. (2.6) is not restricted to systems in equilibrium, but for a pure state $\Psi(\mathbf{r}_1,\mathbf{r}_2,\ldots,\mathbf{r}_N;t)$, for example, it means an expectation value:

$$\rho_1(\mathbf{r},\mathbf{r}';t) = N\int \mathrm{d}\mathbf{r}_2\,\mathrm{d}\mathbf{r}_3\,\ldots\mathrm{d}\mathbf{r}_N\,\Psi^*(\mathbf{r},\mathbf{r}_2,\ldots,\mathbf{r}_N;t)\Psi(\mathbf{r}',\mathbf{r}_2,\ldots,\mathbf{r}_N;t). \tag{2.7}$$

This flexibility is the power of this definition. Our assumption of spinless particles is, in fact, not necessary, but it simplifies the presentation for our purposes.

Definition 2. *Two or more of the eigenvalues $\{n_i\}$ are of order N, and all the others are of order unity $\leftrightarrow$ Fragmented BEC.*

Definition 3. *None of the eigenvalues $\{n_i\}$ is of order N, and all the others are of order unity $\leftrightarrow$ No BEC.*

Alternatively, we may look at the limit of $\hat{\rho}_1$ at infinity [76]. We write

$$\lim_{|\mathbf{r}-\mathbf{r}'|\to\infty}\rho_1(\mathbf{r},\mathbf{r}';t) = N_0\psi^*(\mathbf{r},t)\psi(\mathbf{r}',t). \tag{2.8}$$

Definition 4. *If $\psi(\boldsymbol{r}',t)\neq 0$, the system exhibits BEC and we identify $\psi(\boldsymbol{r}',t)$ with the order parameter. We say there is off-diagonal long-range order.*

2.2 Gross-Pitaevskii Mean-Field Theory

In this Section, we discuss explicitly how the condensation of a gas of bosons in the presence of inter-particle interactions arises. To understand this result, however, we will first revisit the condensation of non-interacting bosons (cf. Sec. 2) more rigorously, after which we can simply 'switch on' the interactions and apply the tools we have built for the non-interacting case.

To begin, let us consider the second-quantised Hamiltonian

$$\hat{H} = \int \mathrm{d}^d\mathbf{r}\ \hat{\psi}^\dagger(\mathbf{r})(\hat{H}_0 - \mu)\hat{\psi}(\mathbf{r}) + \frac{g}{2}\int \mathrm{d}^d\mathbf{r}\ \hat{\psi}^\dagger(\mathbf{r})\hat{\psi}^\dagger(\mathbf{r})\hat{\psi}(\mathbf{r})\hat{\psi}(\mathbf{r}), \tag{2.9}$$

where we have assumed repulsive (attractive) contact inter-particle interactions described by the coupling $g > 0$ (< 0), and introduced the chemical potential μ as a Lagrange multiplier to incorporate the boundary condition that the number of particles N is conserved. The one-body operator is given by $\hat{H}_0 = \hat{\mathbf{p}}^2 + \hat{V}$, where $\hat{V}$ is the external potential felt by the atoms individually. For clarity, we have and will set $\hbar = 2m = 1$. The Hamiltonian (2.9) contains the conservative physics of spinless (single-component) bosons in a d-dimensional system, which includes phenomena such as BEC and superfluidity, superconductivity, quantum vortices, and a Mott insulator state (for a review, see e.g. Refs. [8, 19, 72, 77–81]). Notice that while this Hamiltonian is an exact description of the contact-interaction physics, even the simplified contact interactions will necessitate approximations in practice.

How, then, does the Bose-Einstein condensation of a non-interacting system of N spinless bosons at a finite temperature T arise from the Hamiltonian (2.9)? To see this, let us first perform a Wick rotation $t \to -\mathrm{i}\tau$ into imaginary time τ, and then consider the quantum partition function[4] $Z = \int \mathcal{D}(\psi^*, \psi)\mathrm{e}^{-S[\psi^*,\psi]}$, where (see Refs. [78, 79])

$$S[\psi^*, \psi] = \int \mathrm{d}^d\mathbf{r} \int_0^\beta \mathrm{d}\tau\ \left[\psi^*(\mathbf{r},\tau)(\partial_\tau + \hat{H}_0 - \mu)\psi(\mathbf{r},\tau) + \frac{g}{2}|\psi(\mathbf{r},\tau)|^4\right], \tag{2.10}$$

where ψ is a complex field with a periodic boundary condition $\psi(\mathbf{r},\beta) = \psi(\mathbf{r},0)$. Here $\beta \equiv 1/(k_\mathrm{B}T)$. If we also switch off the external potential so that we have $g = V = 0$, and choose the diagonal basis of the one-body

[4] For a review of coherent-state Feynman path integrals, see e.g. Refs. [78, 79, 82]. The power of the coherent-state path integral approach is the direct intuitive connection to quantum mechanics. Among other things, it also paves the way for Monte Carlo methods [83].

Hamiltonian $\hat{H}_0$, we get in the frequency (momentum) domain

$$\begin{aligned} Z &= \int \mathcal{D}(\psi^*, \psi) \, \exp\left[-\sum_{mn} \psi^*_{mn}(-\mathrm{i}\omega_n + \epsilon_m - \mu)\psi_{mn} \right] \\ &= \prod_{mn} \beta(-\mathrm{i}\omega_n + \epsilon_m - \mu)^{-1}, \end{aligned} \tag{2.11}$$

where $\{\omega_n\}$ are the Matsubara frequencies (for bosons $\omega_n = 2n\pi/\beta$, $n \in \mathbb{Z}$), and the $\{\epsilon_m\}$ are the eigenvalues considered already in Sec. 2. The last equality follows after evaluating the complex Gaussian integrals (exactly). In the path integral language, we can see that the requirement of $\mu \leq 0$ (if $\epsilon_m \geq 0$ and $\epsilon_0 = 0$) ensures that all the weights in the action have the correct sign.

Knowing the partition function, we may compute various quantities using the potential[5] $\Theta = -k_\mathrm{B} T \ln(Z)$. Therefore, using Eq. (2.11), the average number of particles in the system at temperature T and chemical potential μ, N, is given by the relation

$$N \equiv -\frac{\partial \Theta}{\partial \mu} = k_\mathrm{B} T \sum_{mn} \frac{1}{\mathrm{i}\omega_n - \epsilon_m + \mu} = \sum_m n_m(\mu, T), \tag{2.12}$$

where the last equality follows after carrying out the Matsubara frequency summation[6]; in other words, $n_i(\mu, T) = \left[\mathrm{e}^{(\epsilon_i - \mu)/(k_\mathrm{B} T)} - 1\right]^{-1}$ is the Bose-Einstein distribution [cf. Eq. (2.2)]. Starting from the many-body Hamiltonian (2.9), we have arrived at the Bose-Einstein distribution, which we have already considered in Sec. 2 in terms of the non-interacting gas of bosons condensing below the critical temperature T_c [see Eq. (2.4)].

As we have noted, the ground state ϵ_0 is a problem when it equals to μ (i.e. at $T \leq T_\mathrm{c}$). In the path integral, the action for the zero Matsubara component ψ_{00} vanishes [see Eq. (2.11)], and Eq. (2.12) does not accommodate the ground state population N_0 correctly. We rectify the problem as in Sec. 2 by adding the ground state population by hand into the action using ψ_0 (recall at $T \leq T_\mathrm{c}$, $\mu = 0$) as a Lagrange multiplier fixing the total number of particles (see Ref. [78]):

$$S[\psi^*, \psi] \to -\beta \psi_0^* \psi_0 \mu + \sum_{m>0,n} \psi^*_{mn}(-\mathrm{i}\omega_n + \epsilon_m - \mu)\psi_{mn}. \tag{2.13}$$

[5] In fact, Θ is the potential of the grand canonical ensemble. The reservoir is the condensate fraction with a macroscopic occupancy. It can afford to exchange particles with the excited states (in essence the Bogoliubov c-number approximation for operators); in equilibrium, we assume that the system of the excited states is described by the grand canonical ensemble with temperature T and chemical potential μ.

[6] There exists a neat way to evaluate sums of the form $\sum_n h(\omega_n)$, where h is some function of ω_n, by contour integration. For details, see e.g. Ref. [78].

Repeating the same procedure as in Eqs. (2.11) and (2.12), we obtain

$$N = \psi_0^* \psi_0 + N_\mathrm{e}, \tag{2.14}$$

where $N_0 = |\psi_0|^2$ is the number of condensed particles.

Having warmed up with the non-interacting toy model, let us then consider non-zero interactions g. This brings both good news and bad news: the zero-energy ground state will not require any special attention [cf. Eq. (2.13)] (good), but exact evaluation of the field integral is no longer possible [cf. Eq. (2.11)] (bad).

Let us this time consider the normal-time quantum partition function $Z = \int \mathcal{D}(\psi^*, \psi) \mathrm{e}^{\mathrm{i}S[\psi^*,\psi]}$ at $T = 0$, where [see e.g. Ref. [79] or cf. Eq. (2.10)]

$$S[\psi^*, \psi] = \int \mathrm{d}^d\mathbf{r}\, \mathrm{d}t \left[\mathrm{i}\psi^*(\mathbf{r},t)(\partial_t + \mathrm{i}\hat{H}_0 - \mathrm{i}\mu)\psi(\mathbf{r},t) - \frac{g}{2}|\psi(\mathbf{r},t)|^4 \right]. \tag{2.15}$$

The presence of the interactions[7] prevents exact evaluation of the field integral, and we must turn to saddle-point analysis (also known as the principle of stationary action). It is customary to call the solution of the equation of stationary phase the *mean-field*. The result is the time-dependent *Gross-Pitaevskii equation* (GPE) for $\psi(\mathbf{r}, t)$:

$$\boxed{\mathrm{i}\frac{\partial\psi}{\partial t} = -\nabla^2\psi + V(\mathbf{r},t)\psi + g|\psi|^2\psi,} \tag{2.16}$$

where we have scaled the chemical potential away.

If we assume that $\hat{H}_0 = \hat{\mathbf{p}}^2$, i.e. particles in free space, the ground state is simply a time-independent zero-momentum state with uniform density over all space. In this case, the principle of stationary action gives

$$\psi\left(-\mu + g|\psi|^2\right) = 0, \tag{2.17}$$

which has two solutions: $\psi = 0$ (which is the only solution when $\mu < 0$, i.e. no condensation) and $|\psi| = \sqrt{\mu/g}$, which minimises the energy functional corresponding to Eq. (2.16) when $\mu > 0$. The latter solution shows how BEC arises as a quantum phase transition and is an example of spontaneously broken U(1) symmetry[8]. The associated Goldstone mode is linked to superfluidity with massless collective phase fluctuations. For this phenomenon,

[7] Note that in the presence of inter-particle interactions, the chemical potential μ can be positive (cf. Sec. 2).

[8] As we only specify the modulus, the condensate must pick a phase rather arbitrarily. Note the similarity to the Higg's mechanism; the Universe prefers that the Higg's field assumes a non-zero value over all of space (instead of the $\psi = 0$ solution).

we need the next order in the Bogoliubov theory, which in the path integral formalism means considering quadratic fluctuations around the path of stationary phase.

What about collisions of the atoms in the condensate? In general, the collision and scattering of two particles is a complicated process. Here we simply quote the result (see e.g. Ref. [8] for more details) that in the case of dilute Bose or Fermi alkali gases, in the degenerate regime, the inter-particle spacing is so large compared to any range of the interaction energy that considering a contact interaction (for $g > 0$ at least [84]), and furthermore the relative state of the two colliding atoms to be s-wave only meaning $l = 0$, where l is the relative orbital angular momentum, is an excellent approximation. The effective coupling is then in three dimensions

$$g = 8\pi N a_{\mathrm{s}}, \tag{2.18}$$

where a_{s} is the s-wave scattering length. With N included in g, the wave function ψ is normalised to unity.

In the case of a harmonically confined quasi-two-dimensional condensate whereby the z-direction is tightly trapped [85] to the corresponding harmonic oscillator ground state[9], the condensate is projected onto the xy-plane and we obtain an effective coupling

$$g \to C_{2\mathrm{D}} = \frac{4\sqrt{\pi} N a_{\mathrm{s}}}{a_{\mathrm{z}}}. \tag{2.19}$$

Note that to get this result, and henceforth in this Thesis, we work in a dimensionless basis by measuring time, length and energy in terms of ω_{r}^{-1}, $a_{\mathrm{r}} = \sqrt{\hbar/(2m\omega_{\mathrm{r}})}$ and $\hbar\omega_{\mathrm{r}}$ respectively, where ω_{r} is the angular frequency of the trap in the r-direction. This basis is equivalent to setting $\omega_{\mathrm{r}} = \hbar = 2m = 1$. The corresponding GPE is still given by Eq. (2.16), but with Eq. (2.19), and ψ is understood to be a two-dimensional wave function.

To conclude this Section, we introduce the concept of the healing length ξ, which is an important characteristic length scale of condensates (or superfluids in general). It is the distance over which the condensate wave function recovers and tends to its bulk value when subjected to a localised perturbation, like a rigid wall, dark soliton (see Sec. 2.2.1), or a vortex core. The spatial extent of ξ is determined by the potential penalty[10] for deviating from the broken symmetry U(1) ground state being comparable to the gain from

[9] $\omega_{\mathrm{z}} \gg \omega_{\mathrm{x,y}}$ and $a_{\mathrm{z}} = \sqrt{\hbar/(2m\omega_{\mathrm{z}})} \ll \xi$, where a_{z} is the characteristic trap length in the z-direction and ξ is the healing length (see below), and where $\omega_{\mathrm{x,y,z}}$ are the corresponding angular trapping frequencies. Under cylindrical symmetry we set $\omega_{\mathrm{r}} \equiv \omega_{\mathrm{x}} = \omega_{\mathrm{y}}$.

[10] Recall the solution $\psi = 0$ was higher in energy than $\psi = \sqrt{\mu/g}$.

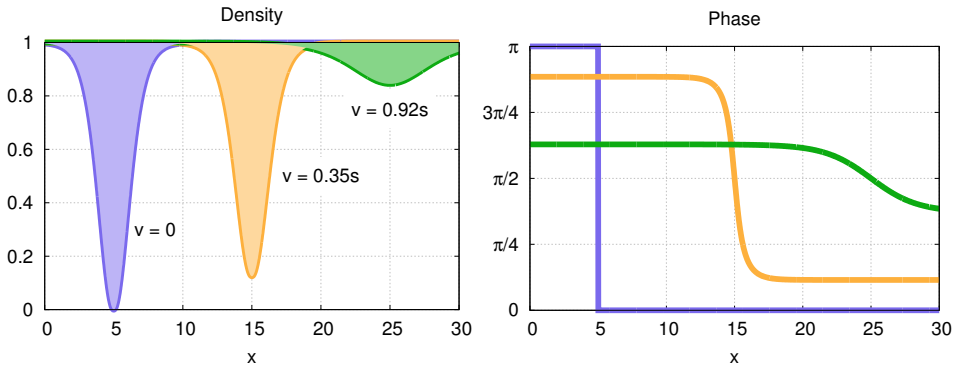

Figure 2.1: The density (left panel) and phase (right panel) profiles of three dark solitons with different speeds [see Eq. (2.22)]. When $v = s$, the speed of sound, the soliton is indistinguishable from the background, and vanishes as phonons. Here $n_0 = g = 1$.

avoiding the diverging kinetic energy at the defect core[11]. Therefore, ξ is determined by $\mu = g|\psi|^2 = \hbar^2/(2m\xi^2) = 1/\xi^2$, viz.:

$$\xi = \frac{1}{\sqrt{8\pi n_0 a_s}}, \tag{2.20}$$

where $n_0 = N|\psi|^2$, the uniform bulk density. For a Bose alkali gas $\xi \simeq 0.5\,\mu$m [86], and in particular, is large[12] compared to the inter-particle separation. This result is in contrast to superfluid helium, where ξ is much smaller, which is another reason why atomic alkali BECs are experimentally attractive.

2.2.1 Dark Solitons and Quantised Vortices

Assuming $V(\mathbf{r}, t) = 0$ in Eq. (2.16) and considering a one-dimensional system, we obtain the nonlinear Schrödinger equation (NLS), which is an integrable soliton equation[13]. The nonlinearity ($g \neq 0$) makes it possible to support

[11] As we will see, the dark soliton corresponds to a phase step of π, and the continuity of the wave function forces the density to vanish, with a potential penalty (see Footnote 10). Similarly, vortices [81] correspond to point-phase singularities. Moving dark solitons correspond to a smooth change in the phase, but the phase gradient, and hence the kinetic energy, is still large.

[12] The vortex core of an alkali BEC would easily house an *Escherichia coli* bacterium [87].

[13] General properties of integrable soliton equations (such as the NLS) include in addition to being nonlinear, the existence of many-soliton solutions (see Sec. 2.2.2), a Lax pair, infinitely many conserved quantities, and the inverse scattering method (a nonlinear generalisation of the Fourier transform) [45].

dark and bright solitons; the equation

$$\mathrm{i}\psi_t = -\psi_{xx} + g|\psi|^2\psi, \tag{2.21}$$

where $g > 0$, has a grey (moving dark) soliton solution (see Fig. 2.1)

$$\boxed{\psi = \sqrt{n_0}\left[\mathrm{i}\frac{v}{s} + \sqrt{1-\frac{v^2}{s^2}}\tanh\left(\sqrt{1-\frac{v^2}{s^2}}\frac{x-vt}{\sqrt{2}\xi}\right)\right]\mathrm{e}^{-\mathrm{i}tgn_0},} \tag{2.22}$$

where v is the speed of the soliton, $s = \sqrt{2n_0 g}$ is the speed of sound, and n_0 is the bulk density, as can be verified by direct substitution (for a derivation see Sec. 2.2.2). If $g < 0$, the solitons are bright, but we will not consider them here. It should be noted that a localised travelling-wave solution is not a soliton in itself - we also need elastic scattering between the solitary waves. If $v = 0$, the solution in Eq. (2.22) is called a *dark soliton*, and the passage of time in the system shows only in the dynamical phase.

In the snake instability, the dark soliton stripe decays into an array of vortex-antivortex pairs (see Sec. 5.1). Let us here define what we mean by a vortex in a BEC. In a spinless BEC, the fluid flow is irrotational, i.e. the vorticity vanishes, as the superfluid velocity is the gradient of the phase S:

$$\nabla \times \mathbf{v} = \frac{\hbar}{m}\nabla \times \nabla S = 0, \tag{2.23}$$

where we have temporarily reintroduced $\hbar$ and m, and where the last equality holds only in a simply connected region, and if the phase S has no singularities. As the wave function must be continuous, an integration along a closed contour encompassing a hole (e.g. on toroidal geometry) or a phase singularity must result in the observation that the phase can only change by an integer multiple of 2π:

$$\int \nabla \times \mathbf{v} \cdot \mathrm{d}\mathbf{S} = \oint \mathbf{v} \cdot \mathrm{d}\mathbf{l} = \frac{h}{m}\ell, \qquad \ell \in \mathbb{Z} \tag{2.24}$$

showing that the circulation is quantised[14] in units of h/m. We can see that if the singularity is on the z-axis, then $\nabla \times \mathbf{v} = \frac{\ell h}{m}\delta^2(\mathbf{r}^{(2)})\hat{\mathbf{e}}_z$, where $\mathbf{r}^{(2)} = x\hat{\mathbf{e}}_x + y\hat{\mathbf{e}}_y$ is a two-dimensional vector, and δ^2 is the two-dimensional delta function. These singularities are the quantised vortices (or vortex lines

[14] Circulation need not be quantised if the atoms have an internal degree of freedom, e.g. spin, which allows for non-singular textures in the presence of angular momentum. See e.g. the Mermin-Ho vortices in superfluid ^{3}He [88] and spinor BECs [89].

in three dimensions), with the winding number ℓ corresponding to a vortex of charge $h\ell/m$.

A *vortex*, then, is a field configuration of non-zero ℓ. The vortex is stable in the sense that the field cannot be continuously deformed to the ground state characterised by a lack of vortices - this is obvious to anyone who has ever played with a band of rubber wound around a cylinder or tried to make a doughnut out of a pancake without puncturing a hole or making new connections. In this sense, the vortex is a topological defect, and its particular location in the condensate is irrelevant.

We can say that topological defects (such as quantised vortices) exist and persevere because of the topology of the order parameter describing the broken symmetry BEC state [90]. Specifically, in the path integral formalism, we must extend the path integral by hand to spaces that are not simply connected, which creates separate classes of trajectories categorised by their winding number. To see this, consider a toy example of a particle on a ring, that is, with the Hamiltonian $\hat{H}_0 = -\frac{1}{2I}\frac{\partial^2}{\partial\theta^2}$, where $\theta \in [0, 2\pi]$ is measuring the position of the particle, and I is the moment of inertia. The eigenvalues of $\hat{H}_0$ are $\ell^2/(2I)$, $\ell \in \mathbb{Z}$; the path integral representation of the partition function $Z = \sum_{\ell=-\infty}^{\infty} \exp\left[-\beta\ell^2/(2I)\right]$ is[15]

$$Z = \int_0^{2\pi} \mathrm{d}\theta_0 \sum_{\ell=-\infty}^{\infty} \int_{\theta(0)=\theta_0}^{\theta(\beta)-\theta(0)=2\pi\ell} \mathcal{D}\theta(\tau) \exp\left[-\frac{I}{2}\int_0^{\beta} \mathrm{d}\tau\dot{\theta}^2\right]. \tag{2.25}$$

Notice the requirement to categorise the trajectories into (homotopy) classes specified by the winding number ℓ.

The Euler-Lagrange equations for the action of the system give $\ddot{\theta} = 0$, which subject to the boundary conditions has a family of solutions characterised by the parameter ℓ: $\theta_\ell(\tau) - \theta_\ell(0) = 2\pi\ell\tau/\beta$. It is not possible to change ℓ by a continuous deformation of θ_ℓ (the trajectory) because the boundary conditions are fixed in the path integral, the net ℓ is always the same. A vortex can only be destroyed by tearing up the topology at the edge, for example, where the vortex decays into elementary excitations [91]. Similarly, vortices are created from surface waves by gluing the topology up at the edge of the condensate, or by means of e.g. the snake instability (see Sec. 5.1).

[15] We can e.g. use the well-known results $\left\langle \theta_f \middle| \mathrm{e}^{-\mathrm{i}\hat{H}_0 t} \middle| \theta_i \right\rangle = \int_{\theta(0)=\theta_i}^{\theta(t)=\theta_f} \mathcal{D}\theta\, \mathrm{e}^{\mathrm{i}\int_0^t \mathrm{d}t' I\dot{\theta}^2/2}$, and $Z = \int \mathrm{d}\theta \left\langle \theta \middle| \mathrm{e}^{-\beta\hat{H}_0} \middle| \theta \right\rangle$ (Wick rotated).

2.2.2 Dark Soliton Solution by the Hirota Direct Method

The soliton solutions of the NLS have been exactly solved using the Inverse Scattering Transform [45] (a so called Zakharov-Shabat spectral problem [92, 93]) and the Hirota Direct Method [46], recovering the previously found soliton solutions [94]. In this section, we show in detail how the dark soliton solution is derived using the Hirota method.

Setting $g = 1$ in Eq. (2.16)[16], we obtain the NLS in the following (canonical) form:

$$\mathrm{i}\psi_t = -\psi_{xx} + |\psi|^2\psi. \tag{2.26}$$

This can be brought to the Hirota bilinear form using the transformation $\psi = w/f$, where $w \in \mathbb{C}$ and $f \in \mathbb{R}$:

$$\begin{cases} (\mathrm{i}D_t + D_x^2 - \lambda)\, w \cdot f = 0 \\ (D_x^2 - \lambda)\, f \cdot f = -|w|^2, \end{cases} \tag{2.27}$$

where λ is the decoupling constant and D is the well-known Hirota bilinear operator:

$$D_x^n D_t^m w \cdot f \equiv (\partial_x - \partial_{x'})^n (\partial_t - \partial_{t'})^m w(x,t) f(x',t')|_{x=x',t=t'}. \tag{2.28}$$

Following the Hirota direct method, we write the ansatz

$$w = \sum_{j=0}^{\infty} \epsilon^j w^{(j)}, \qquad f = 1 + \sum_{j=1}^{\infty} \epsilon^j f^{(j)}, \tag{2.29}$$

and substitute it in Eq. (2.27). Equating like terms results in a collection of recurrence relations for $f^{(j)}$ and $w^{(j)}$:

$$\mathcal{O}(1) \begin{cases} \mathrm{i}w_t^{(0)} + w_{xx}^{(0)} = \lambda w^{(0)} \\ w^{(0)}\bar{w}^{(0)} = \lambda, \end{cases} \tag{2.30}$$

$$\mathcal{O}(\epsilon) \begin{cases} \mathrm{i}w_t^{(1)} + w_{xx}^{(1)} = -(\mathrm{i}D_t + D_x^2) w^{(0)} \cdot f^{(1)} + \lambda(w^{(0)} f^{(1)} + w^{(1)}) \\ 2f_{xx}^{(1)} = -(w^{(0)}\bar{w}^{(1)} + \bar{w}^{(0)} w^{(1)}) + 2\lambda f^{(1)}, \end{cases} \tag{2.31}$$

$$\mathcal{O}(\epsilon^2) \begin{cases} \mathrm{i}w_t^{(2)} + w_{xx}^{(2)} = -(\mathrm{i}D_t + D_x^2)(w^{(0)} \cdot f^{(2)} + w^{(1)} \cdot f^{(1)}) \\ \qquad\qquad + \lambda(w^{(0)} f^{(2)} + w^{(1)} f^{(1)} + w^{(2)}) \\ 2f_{xx}^{(2)} = -D_x^2 f^{(1)} \cdot f^{(1)} - (w^{(0)}\bar{w}^{(2)} + w^{(1)}\bar{w}^{(1)} + \bar{w}^{(0)} w^{(2)}) \\ \qquad\qquad + \lambda(2f^{(2)} + f^{(1)2}), \end{cases} \tag{2.32}$$

[16] $g = -1$ (in general negative) is needed to obtain bright solitons.

and so on, where the bar denotes complex conjugate. It is clear from Eq. (2.30) that $\lambda > 0$, and we can take $w^{(0)} = \sqrt{\lambda}\mathrm{e}^{\mathrm{i}(k_0 X - \omega_0 T + w_0)}$ if $\omega_0 = k_0^2 + \lambda$. If the background is at rest ($k_0 = 0$), it follows from our scaling of units that $\omega_0 = 1$.

The one-soliton solution (1SS) is built perturbatively by $w^{(1)} = C w^{(0)} f^{(1)}$, $f^{(1)} = \mathrm{e}^{\eta_1}$, and all the rest vanishing, where $\eta_1 = kX - \omega T + \eta_0$, and $C \in \mathbb{C}$; $k, \omega \in \mathbb{R}$. Equations (2.31) and (2.32) impose restrictions on the parameters, and we obtain

$$\mathcal{O}(\epsilon) \begin{cases} (-\mathrm{i}\omega + k^2 + 2\mathrm{i}k_0 k)C = 2k_0^2 + 2\lambda - \mathrm{i}\omega + 2\mathrm{i}k_0 k - k^2 \\ \mathrm{Re}\, C = 1 - k^2/\lambda, \end{cases} \tag{2.33}$$

$$\mathcal{O}(\epsilon^2) \begin{cases} \omega_0 = k_0^2 + \lambda \\ |C|^2 = 1, \end{cases} \tag{2.34}$$

so that

$$C = \frac{\sqrt{2\lambda - k^2} + \mathrm{i}k}{\sqrt{2\lambda - k^2} - \mathrm{i}k}, \qquad \omega = k(2k_0 - \sqrt{2\lambda - k^2}). \tag{2.35}$$

We can see that the lower equation in Eq. (2.27) gives the phase factor while the upper equation gives the dispersion relation. Setting $\lambda = 1$, the 1SS obtains the form

$$\psi_{1\mathrm{SS}} = \frac{1 + C\mathrm{e}^{\eta_1}}{1 + \mathrm{e}^{\eta_1}} \mathrm{e}^{\mathrm{i}(k_0 x - \omega_0 t + w_0)}, \tag{2.36}$$

which is equivalent to Eq. (2.22). The remarkable advantage of the Hirota method is that the N-soliton solution to the NLS [see Eq. (2.26)] can be written down by essentially continuing the series in Eq. (2.29).

2.3 Bogoliubov-de Gennes Theory

In order to obtain the GPE [see Eq. (2.16)], we only considered the path of $\psi(\mathbf{r}, t)$ in the action [see Eq. (2.15)]. In general, also the fluctuations around the mean-field matter. Substituting $\psi(\mathbf{r}, t) \to \psi(\mathbf{r}, t) + \delta\psi$ in the action (2.15), we obtain

$$S[\psi^*, \psi] = S_0 + \int \mathrm{d}^d\mathbf{r}\, \mathrm{d}t \left\{ \mathrm{i}\psi^* \hat{A}\delta\psi + \mathrm{i}\delta\psi^* \hat{A}\psi - \frac{g}{2}\left[2|\psi|^2(\psi^*\delta\psi + \delta\psi^*\psi)\right] \right\}, \tag{2.37}$$

where $\hat{A} \equiv \partial_t + \mathrm{i}\hat{H}_0 - \mathrm{i}\mu$, and S_0 is the action (2.15). We have ignored contributions $\sim \mathcal{O}(|\delta\psi|^2)$, which means that $\delta\psi$ must be small. The stationary action principle $\delta S[\psi^*, \psi]/\delta\psi^* = 0$ leads to the GPE (the S_0 term), and

$$(\mathrm{i}\partial_t - \hat{H}_0 + \mu)\delta\psi - g(2|\psi|^2\delta\psi + \psi^2\delta\psi^*) = 0. \tag{2.38}$$

This equation couples $\delta\psi$ and $\delta\psi^*$, which are independent variables[17]. We get a second equation by taking the Hermitian conjugate of Eq. (2.38), i.e. using the independent stationary action principle $\delta S[\psi^*,\psi]/\delta\psi = 0$. Note that linearising the GPE around the mean-field solution ψ_0 ($\hat{\psi} = \psi_0 + \delta\hat{\psi}$, where ψ_0 denotes the mean-field satisfying the GPE) gives the same result.

As is customary, we write the fluctuations in terms of amplitudes u and v, such that

$$\psi(\mathbf{r},t) = \mathrm{e}^{-\mathrm{i}\mu t}\left\{\psi_0(\mathbf{r}) + \left[u(\mathbf{r})\mathrm{e}^{-\mathrm{i}\Omega t} + v(\mathbf{r})^*\mathrm{e}^{\mathrm{i}\Omega t}\right]\right\}, \tag{2.39}$$

where $\Omega \in \mathbb{R}$. Considering two-dimensional plane polar geometry, we parametrise $\{u,v\}(\mathbf{r}) = \mathrm{e}^{\mathrm{i}q\theta}\{u_q, v_q\}(r)$ [95]. From Eq. (2.38), u and v satisfy the *Bogoliubov-de Gennes equations*:

$$\begin{pmatrix} \mathcal{H} & C_{2\mathrm{D}}\psi_0^2 \\ C_{2\mathrm{D}}(\psi_0^*)^2 & \mathcal{H} \end{pmatrix}\begin{pmatrix} u_q \\ v_q \end{pmatrix} = \Omega_q \begin{pmatrix} u_q \\ -v_q \end{pmatrix}, \tag{2.40}$$

where $\mathcal{H} = -\partial_r^2 - \frac{1}{r}\partial_r + \frac{q^2}{r^2} + V + 2C_{2\mathrm{D}}|\psi_0|^2 - \mu$, and ψ_0 is a self-consistent wave function satisfying the GPE. In general, we have $(\Omega_q - \Omega_{q'}^*)\int \mathrm{d}\mathbf{r}(u_q^* u_{q'} - v_{q'}^* v_q) = 0$. An imaginary eigenvalue Ω_q signifies a dynamical instability, with the characteristic decay time $1/\mathrm{Im}(\Omega_q)$. If all the eigenvalues $\{\Omega_q\}$ are real, the condensate ψ_0 is dynamically stable.

[17] A moment's thought reveals that if ψ changes, so does ψ^*. A natural question is then that how is the partial functional derivative $\delta S[\psi^*,\psi]/\delta\psi^*$ defined, if we cannot assume $\delta\psi$ is constant. One solution is to consider Wirtinger derivatives and write $\psi = x + \mathrm{i}y$, x and y are real and independent, and then $\frac{\partial}{\partial\psi} \equiv \frac{1}{2}\left(\frac{\partial}{\partial x}\Big|_y - \mathrm{i}\,\frac{\partial}{\partial y}\Big|_x\right)$. They satisfy the product rule of ordinary differential operators, $\frac{\partial(\psi^n)}{\partial\psi} = n\psi^{n-1}$, and $\frac{\partial f(\psi^*)}{\partial\psi} = 0$, where f is a Taylor series. The result of these properties is that we can treat ψ and ψ^* as if they are independent variables when taking the differentials.

Chapter 3

Exact Soliton-like Solutions of the Radial GPE

The radial GPE (in dimensionless form) is given by[1]

$$\mathrm{i}\psi_T = -\psi_{RR} - \frac{1}{R}\psi_R + V(R,T)\psi + g|\psi|^2\psi, \tag{3.1}$$

where the order parameter ψ can be, for example, the macroscopic wave function of a Bose-Einstein condensate in an ultra-cold atomic gas setting, or the scalar mean field of a polariton condensate [96] (in the limit of vanishing polariton pumping and decay). Our focus is the former, so that $V(R,T)$ is the external trapping potential of the atoms. We will mainly consider the repulsive case $g = 1$, and our aim is to find exact ring dark soliton solutions to Eq. (3.1), or to show that they do not exist. In particular, in this Chapter, we provide an introduction to Publication I by discussing how one might go about finding soliton solutions to Eq. (3.1).

3.1 Possible Methods for Finding Solutions

Hirota Direct Method

In Sec. 2.2.2, we showed how the planar many-soliton solutions of the NLS equation (2.26) can be obtained by the Hirota direct method. The Hirota direct method is a powerful tool for finding exact soliton solutions, so it is reasonable to try it with Eq. (3.1) as well. However, we note at the start that Eq. (3.1) is not integrable in the sense that it does not pass the Painlevé

[1] Consider $\nabla^2 = \partial_R^2 + \frac{1}{R}\partial_R + \frac{1}{R^2}\partial_\theta^2$ in Eq. (2.16). For consistency with Publication I, we use capital letters for r and t in Eq. (3.1).

test (because $\alpha_1 \neq \alpha_1(t)$, see the next subsection) [97, 98], so it might not be expected that the Hirota method should work.

Setting $V = 0$ and $g = 1$ in Eq. (3.1), and assuming that the same transformation as in Sec. 2.2.2 is the correct choice of bilinearisation, Eq. (3.1) results in the following bilinear form:

$$\begin{cases} \left(\mathrm{i}D_T + D_R^2 + \frac{1}{R}D_R - \lambda\right) w \cdot f = 0 \\ \left(D_R^2 - \lambda\right) f \cdot f = -|w|^2, \end{cases} \tag{3.2}$$

where λ is the decoupling constant, and D is as defined in Eq. (2.28). From the second equation in Eq. (3.2), we obtain

$$-|\psi|^2 = \frac{D_R^2 f \cdot f}{f^2} - \lambda, \tag{3.3}$$

which means that the value of λ is fixed by the limiting behaviour of $|\psi|^2$ at $R \to \{0, \infty\}$, and f. For $|x| \to \infty$ in the case of the planar dark soliton, we obtain in this limit that $|\psi|^2 = \lambda$ [see Eq. (2.27)], and our normalisation convention sets $\lambda = 1$ (see Sec. 2.2.2). Similarly, one would set $\lambda = 0$ for the planar bright soliton. However, following the Hirota direct method and writing the dark 1-soliton ansatz

$$w = w^{(0)} + \epsilon w^{(1)}, \qquad f = 1 + \epsilon f^{(1)} \tag{3.4}$$

as usual, equating like terms upon substitution of Eq. (3.4) in Eq. (3.2) shows that f and w cannot be (sums of) simple exponentials anymore like in the planar case. The Hirota method (with the above bilinearisation) fails to produce solutions to Eq. (3.1).

Combined Point-, Gauge-, and Scale Transformation

The variable R in Eq. (3.1) is strictly positive, so it seems useful to apply the transformation $x = \ln(R)$ and $t = T$, which results in

$$\mathrm{i}\psi_t = -\frac{1}{\mathrm{e}^{2x}}\psi_{xx} + V(x,t)\psi + |\psi|^2\psi. \tag{3.5}$$

From now on we will consider the generalised equation

$$\mathrm{i}\psi_t = -\alpha_1(x,t)\psi_{xx} + \alpha_2(x,t)\psi + \alpha_3(x,t)|\psi|^2\psi, \tag{3.6}$$

where α_{1-3} are some functions of x and t, and consider our case, Eq. (3.1), as the following special case:

$$\alpha_1(x,t) = \frac{1}{\mathrm{e}^{2x}}, \qquad \alpha_2(x,t) = V(x,t), \qquad \alpha_3(x,t) = 1. \tag{3.7}$$

Another possible method of solution is a general transformation [99, 100] combining point-, gauge- or scale-transformations, i.e. transformations that leave Eq. (3.6) form-invariant, but possibly changing the functions α_{1-3} into different ones. The hope is to obtain another equation that we know the solutions for, but the result is the same as in the previous subsection: it turns out that Eqs. (2.26) and (3.1) are not connected by such a transformation. To see why, we apply the general transformation

$$\psi(x,t) = \rho(x,t)\mathrm{e}^{\mathrm{i}\varphi(x,t)}\phi[\eta(x,t),\gamma(x,t)], \tag{3.8}$$

where ρ, φ, η, and γ are real functions to be determined so that this transformation connects Eq. (3.6) and

$$\mathrm{i}\phi_\gamma = -\phi_{\eta\eta} + G|\phi|^2\phi \tag{3.9}$$

for some constant G. Using symbolic computation with $\alpha_1(x,t) = \mathrm{e}^{-2x}$, we obtain the following requirements:

$$\alpha_2 = \frac{1}{4}\mathrm{e}^{-2x} + \gamma_1(t)\mathrm{e}^{2x} + \gamma_2(t)\mathrm{e}^{x} + \gamma_3(t), \tag{3.10a}$$

$$\alpha_3 = \gamma_4(t)\mathrm{e}^{x}, \tag{3.10b}$$

where γ_{1-3} are three functions of time, and γ_4 depends on γ_1 (see below). Because the nonlinear term has a constant coefficient in the radial GPE (3.1), we cannot use the transformation (3.8).

However, if we allow for a radially dependent nonlinearity (e.g. a spatially dependent magnetic trap near a Feshbach resonance), then the transformation can find solutions to the equation

$$\mathrm{i}\psi_t = -\psi_{RR} - \frac{1}{R}\psi_R + \left[\frac{1}{4R^2} + \gamma_1(t)R^2 + \gamma_2(t)R + \gamma_3(t)\right]\psi + G\gamma_4(t)R|\psi|^2\psi. \tag{3.11}$$

Scaling the wave function by $\psi \to \sqrt{R}\psi$ results in the equation

$$\mathrm{i}\psi_t = -\psi_{RR} + \left[\gamma_1(t)\left(R + \frac{\gamma_2(t)}{2\gamma_1(t)}\right)^2 - \frac{\gamma_2^2(t)}{4\gamma_1(t)} + \gamma_3(t)\right]\psi + G\gamma_4(t)|\psi|^2\psi, \tag{3.12}$$

where we have rewritten the potential to emphasise the toroidal geometry. In particular, Eq. (3.9) is connected to Eq. (3.12) by the transformation

$$\psi(R,t) = \rho(R,t)\mathrm{e}^{\mathrm{i}\varphi(R,t)}\phi[\eta(R,t),\gamma(R,t)], \tag{3.13}$$

where

$$\rho(R,t) = \pm\sqrt{\alpha\beta_1(t)}, \tag{3.14a}$$
$$\eta(R,t) = \beta_1(t)R + \beta_2(t), \tag{3.14b}$$
$$\gamma(R,t) = \delta + \int^t \beta_1^2(t')\,\mathrm{d}t', \tag{3.14c}$$
$$\varphi(R,t) = \beta_3(t) - \frac{\dot\beta_1(t)R^2 + 2\dot\beta_2(t)R}{4\beta_1(t)}, \tag{3.14d}$$

where α and δ are constants, β_{1-3} are arbitrary real functions of time, and

$$\gamma_1(t) = \frac{\ddot\beta_1(t)}{4\beta_1(t)} - \frac{\dot\beta_1^2(t)}{2\beta_1^2(t)}, \tag{3.15a}$$
$$\gamma_2(t) = \frac{\ddot\beta_2(t)}{2\beta_1(t)} - \frac{\dot\beta_1(t)\dot\beta_2(t)}{\beta_1^2(t)}, \tag{3.15b}$$
$$\gamma_3(t) = -\dot\beta_3(t) - \frac{\dot\beta_2^2(t)}{4\beta_1^2(t)}, \tag{3.15c}$$
$$\gamma_4(t) = \frac{\beta_1(t)}{\alpha}. \tag{3.15d}$$

For example, the dark soliton solution $\phi(\eta,\gamma) = \tanh\left[\sqrt{\frac{G}{2}}\eta\right]\mathrm{e}^{-\mathrm{i}G\gamma}$ of Eq. (3.9) gives the solution

$$\begin{aligned}\psi(R,t) = \pm\sqrt{\alpha\beta_1(t)}\exp\left[\mathrm{i}\left(\beta_3(t) - \frac{\dot\beta_1(t)R^2 + 2\dot\beta_2(t)R}{4\beta_1(t)}\right)\right] \\ \times\tanh\left\{\sqrt{G/2}\,[\beta_1(t)R + \beta_2(t)]\right\}\mathrm{e}^{-\mathrm{i}G\left[\delta + \int^t \beta_1^2(t')\,\mathrm{d}t'\right]}\end{aligned} \tag{3.16}$$

of Eq. (3.12) with the time-dependent functions as given in Eqs. (3.15a)-(3.15d). For definiteness, we can make particular choices of the functions β_{1-4} to obtain solutions, for example:

$$\psi(R,t) = \pm\sqrt{t}\tanh\left(\sqrt{\frac{G}{2}}tR\right)\exp\left[-\mathrm{i}\left(\frac{R^2}{4t} + \frac{G}{3}t^3\right)\right] \tag{3.17}$$

solves

$$\mathrm{i}\psi_t = -\psi_{RR} - \frac{R^2}{2t^2}\psi + Gt|\psi|^2\psi, \tag{3.18}$$

and

$$\psi(R,t) = \pm\mathrm{e}^{\frac{t}{2}}\tanh\left[\sqrt{\frac{G}{2}}\mathrm{e}^t(R-2)\right]\exp\left[-\mathrm{i}\left(\frac{R^2}{4} - R + \frac{G}{2}\mathrm{e}^{2t}\right)\right] \tag{3.19}$$

solves

$$\mathrm{i}\psi_t = -\psi_{RR} - \frac{1}{4}(R-2)^2\psi + G\mathrm{e}^t|\psi|^2\psi. \tag{3.20}$$

We can see from Eqs. (3.14a) and (3.15a) that a non-zero R^2 term in the potential requires nontrivial time dependence in $\beta_1(t)$, making these solutions depend on time in a complicated way. In Sec. 3.2 and in more detail in Publication I, we present exact soliton-like stationary solutions to Eq. (3.1).

3.2 Ring Dark Soliton-like Solution

We can make progress by considering the similarity transformation method [101], i.e. the following ansatz for Eq. (3.6):

$$\psi(x,t) = \rho(x,t)\mathrm{e}^{\mathrm{i}\varphi(x,t)}\phi(\eta(x,t)), \tag{3.21}$$

where $\rho \in \mathbb{R}^+$ and $\{\varphi, \eta\} \in \mathbb{R}$ are some functions to be determined, and $\phi(\eta)$ is assumed to satisfy

$$-\phi_{\eta\eta} + h(\eta)\phi + G\phi^3 = 0, \tag{3.22}$$

where G is a constant, and h is an arbitrary function of η. The resulting set of equations and their solution is detailed in Publication I. In the rest of this section, we highlight an interesting soliton-like dark ring solution, corresponding to a particular choice of h.

If $h(\eta) = -\kappa$, then Eq. (3.22) reduces to the NLS equation $\kappa\phi = -\phi_{\eta\eta} + G\phi^3$, and we can construct the following solution to Eq. (3.1) (see Fig. 3.1):

$$\psi(R,T) = R^{-\frac{1}{3}}\sqrt{\kappa}\tanh\left[\frac{3}{2\sqrt{2}}\sqrt{\kappa}(R^{\frac{2}{3}} - R_0^{\frac{2}{3}})\right]\mathrm{e}^{-\mathrm{i}T}, \tag{3.23}$$

where $\kappa > 0$, and the potential is given by

$$V(R) = \frac{1}{9R^2} - \kappa\frac{1}{R^{\frac{2}{3}}} + 1. \tag{3.24}$$

Equation (3.23) describes a stationary soliton-like[2] dark ring of radius R_0. Numerical simulations show that it undergoes the snake instability (see Sec. 5.1)

[2] It has solitonic properties, e.g. the notch is a localised solitary wave, and there is a phase jump by π across the notch. Interestingly, the solution can be written similarly to the Thomas-Fermi approximation; if we write $T \to T - \frac{\theta}{3}$, then $\tilde{\psi}(R,\theta,T) = \sqrt{\frac{\mu-\tilde{V}(R)}{g}}\psi(R,\theta,T)\Big|_{\mu=g=1}$ solves $\mathrm{i}\tilde{\psi}_T = -\tilde{\psi}_{RR} - \frac{1}{R}\tilde{\psi}_R - \frac{1}{R^2}\tilde{\psi}_{\theta\theta} + \tilde{V}(R)\tilde{\psi} + |\tilde{\psi}|^2\tilde{\psi}$, where $\tilde{V}(R) = 1 - \kappa\frac{1}{R^{\frac{2}{3}}}$.

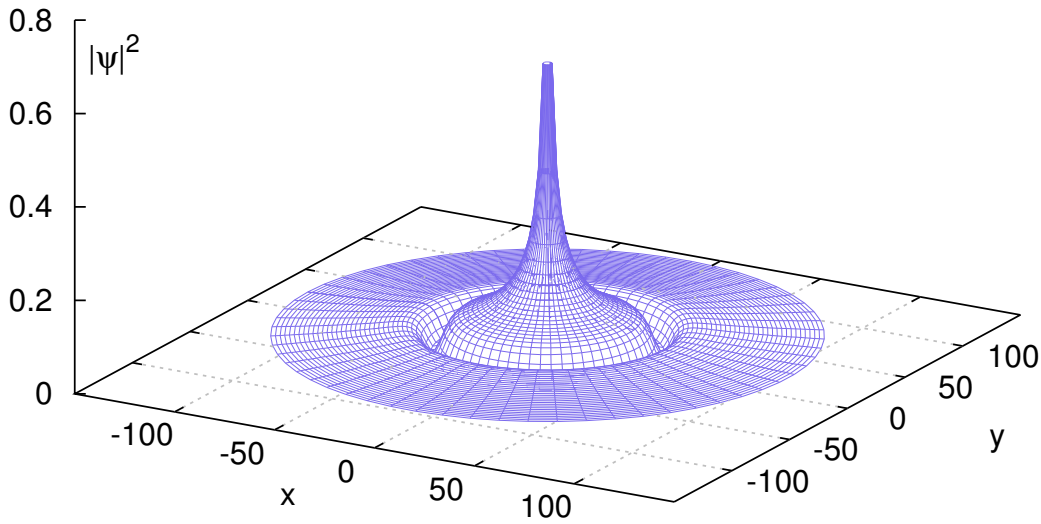

Figure 3.1: The exact soliton-like solution (3.23) of Eq. (3.1) with the potential (3.24). Here $\kappa = 1$ and $R_0 = 50$.

producing a necklace of vortex-antivortex pairs. For $\kappa = 1$, the Bogoliubov-de Gennes equations (2.40) show that the solution is always formally unstable with respect to the $q = 0$ mode, but for $R_0 \lesssim 1.5003$, the $q = 0$ is the only instability mode. Furthermore, in the limit $R_0 \to \infty$, the decay times of the snake instability approach infinity as well, but rather slowly. For details, see Sec. 3.2 of Publication I.

Finally, we draw attention to a recent manuscript [102], where an experimental realisation of Eq. (3.23) has been reported in the case of a polariton condensate. While the central divergence (at $R = 0$) of Eq. (3.23) is strictly speaking unphysical, an experimental polariton condensate setting is dynamical in nature due to the finite lifetime and the need for constant regeneration of the polaritons, and a steady state can sustain polariton flows (making them also more difficult to find). It was suggested in [102] that the solution (3.23) corresponds to a steady state. Therefore, there is no divergence in practice, as the central spot cannot be fed for infinitely long to establish the steady state[3]. Still, it forms a pioneering example of a novel class of *physical singularities* in quantum liquids, with already existing experimental support [102].

[3]Also, when the exciton-polariton density exceeds the Mott critical value, i.e. the excitons start overlapping, the Gross-Pitaevskii treatment breaks down [103].

Chapter 4

Creation of Ring Dark Solitons

We have seen in Chapter 3 that finding exact soliton solutions to Eq. (3.1) is difficult, and the solution (3.23) is not a soliton in the strict mathematical sense (though, the radial GPE (3.1) does not seem to be integrable either, see Sec. 3.1). Can ring dark solitons (RDSs) [68] still be created experimentally in a condensate? To date, RDSs have not been experimentally observed with cold atomic gases, although experiments on optical ring dark solitary waves [67] have been reported [69, 104, 105].

The soliton-like solution (3.23) offers some guidance: a RDS should have a phase step of π (if its radius is not changing) and it should correspond to a radial density node [70, 106]. Therefore, a plausible strategy would seem to be to print an appropriate radial phase step [68], and let the density respond by producing the RDS. Phase imprinting has been used to create planar dark solitons [57, 107, 108]) and optical RDSs [109], and numerical simulations show that the result can indeed be a long-lived radial density node (see Sec. 5.2).

On the other hand, it is also possible to consider the complementary method of density imprinting, whereby we impose a density node and let the phase respond by producing a step, and subsequently the density fully evolve into a RDS. Printing density nodes is possible by e.g. letting two condensates expand over each other producing an interference pattern [110]. When the collisional energy per atom E_c of the two condensates dominates, the interference pattern (in the z-direction) is described by a $\cos^2(kz)$-modulation, where the wavenumber $k^2 = E_c$, but when E_c is comparable to the nonlinear self-energy, it is favourable for the nodes to evolve into dark solitons instead [111–115].

In Publications III and IV, we present two density-imprinting protocols for the experimental creation of RDSs (see Sections 4.1 and 4.2), but focussing on the self-interference of a single condensate. The self-interference fringes

create density nodes in the condensate wave function, which subsequently develop into structures we term RDSs because of their solitonic properties such as their long lifetimes, elastic collisions, and appropriate phase jumps.

The self-interference dynamics of a BEC with repulsive interactions in a hard-wall trap resulting from free expansion and reflection of the BEC has been demonstrated by numerical simulations [116, 117]. The observed phenomena included the formation of soliton-like self-interference fringes both in a 1D box and a 2D disk. When the expanding condensate was initially displaced from the centre of the circular disk, the angular symmetry of the RDSs was broken, and they were observed to decay into vortex-antivortex pairs, in agreement with the snake instability mechanism discussed in Sec. 5.1. These processes are in contrast to our protocols, which involve a time-dependent toroidal double-well potential (see Publication III) and free expansion of a toroidal condensate (see Publication IV). Furthermore, we can fully control the number of RDSs produced in the first protocol.

The protocol of Publication III is based on the (quasi-)adiabatic passage with possible diabatic jumps of the initial state, and the population is transferred from the ground state of the inner well to the outer well [118, 119]. We interpret the observed dynamics in terms of the condensate tunnelling to the outer well and interfering with itself producing nodes. In contrast, it has been shown [120] that the nonlinear eigenstates of a harmonic potential can correspond to dark solitons. In a similar work [121], quantum tunnelling in a double-well has been used to generate dark solitons as well, and the mechanism was explained by direct coupled dynamics of the ground and multiple excited states of the nonlinear system. We find that also the self-interference model gives quantitative predictions (see Sec. 4.2).

Finally, we note that interference is fundamentally a linear process, but the existence of dark solitons depends upon the non-zero (and positive) nonlinearity of the condensate[1]. These two regimes are connected during the time evolution, whereby the initial linear fringes develop into nonlinear dark soliton notches; the process might be described as *nonlinear interference*.

4.1 Self-Interference in a Toroidal Well

Very recently, matter-wave Bessel beams have been experimentally created by letting a toroidally trapped condensate expand freely [122]. The expansion produces a cylindrically symmetric interference pattern that was numerically

[1]Setting $g = 0$ results in Eq. (2.22) reducing to the trivial solution $\psi = 0$ because in the limit as $a_s \to 0$, we have $\mu \to 0$ and $\xi \to \infty$ [see Sec. 2.2 and Eq. (2.20)].

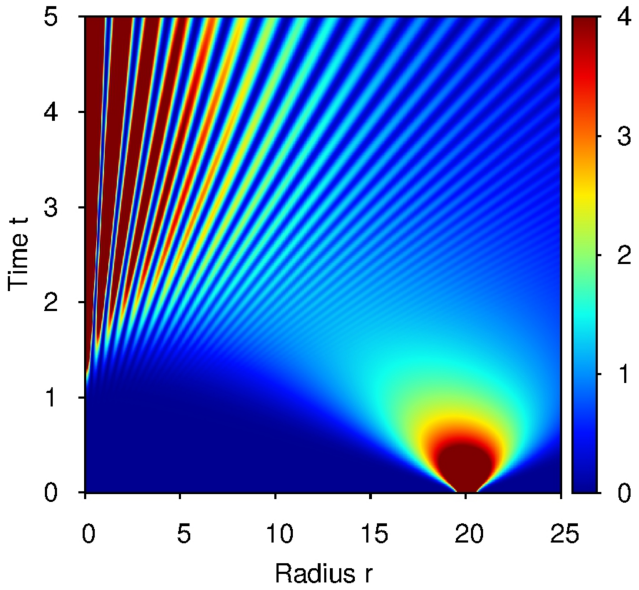

Figure 4.1: Density plot of the free expansion of a toroidal condensate [see Eq. (4.1)]. Here $r_0 = 20$, $\sigma^2 = 0.1$, and the density is in arbitrary units.

observed to correspond to Bessel function modulation. Independently, in Publication IV, we have studied the free expansion of a toroidal condensate of initial radius r_0 theoretically, showing that the expansion dynamics at time t is given to a good approximation by (see Fig. 4.1)

$$\varphi_{\mathrm{G}}(r,t) = \frac{\mathcal{N}\sigma^2}{\sigma^2 - 2\mathrm{i}t} \exp\left(-\frac{r^2 + r_0^2}{2\sigma^2 - 4\mathrm{i}t}\right) I_0\left(\frac{rr_0}{\sigma^2 - 2\mathrm{i}t}\right), \tag{4.1}$$

where I_0 is the modified Bessel function of order 0. The initial ring condensate and its confinement are given by

$$\varphi_{\mathrm{G}}(r,0) = \mathcal{N}\mathrm{e}^{-\frac{(r-r_0)^2}{2\sigma^2}}, \qquad V = \frac{1}{4}\omega^2(r - r_0)^2, \tag{4.2}$$

respectively, where $\mathcal{N}$ is the normalisation, and $\sigma = \sqrt{2/\omega}$.

The argument of I_0 is complex in Eq. (4.1), which gives rise to oscillations and, in particular, shows that the self-interference fringes are given by a Bessel function in a cylindrically symmetric system[2]. If the potential is chosen appropriately after the free expansion, it is possible to create RDSs from (some of) the fringes (see Publication IV for details).

[2]Using the properties of the Bessel functions [123], for $t \gg 1$ in Eq. (4.1) we may write $I_0\left(\frac{rr_0}{\sigma^2 - 2\mathrm{i}t}\right) \approx J_0\left(\frac{rr_0}{2t}\right) \overset{r_0\to\infty}{\sim} \sqrt{\frac{4t}{\pi r r_0}} \cos\left(\frac{rr_0}{2t} - \frac{\pi}{4}\right)$ showing the emergence of the typical $\cos^2$-modulation of interference fringes in the planar limit, where J_0 is the Bessel function of the first kind.

4.2 Self-Interference in a Toroidal Double-Well

In Publication III, we show that if we consider the two-dimensional GPE [see Eqs. (2.16) and (2.19)]

$$\mathrm{i}\psi_t = -\nabla^2\psi + V\psi + C_{2\mathrm{D}}|\psi^2|\psi, \tag{4.3}$$

where the trapping potential V is chosen to be a toroidal double-well consisting of two harmonic wells with time-dependent energy minima $\Delta_i(t)$ and radii $r_i(t)$ $(i = 1, 2)$, it is possible to print a desired number of RDSs onto the toroidal condensate. Specifically,

$$V(r,t) = \begin{cases} V_1(r,t) = \frac{\omega^2}{4}[r - r_1(t)]^2 + \Delta_1(t) & (r \le r_\mathrm{v}) \\ V_2(r,t) = \frac{\omega^2}{4}[r - r_2(t)]^2 + \Delta_2(t) & (r > r_\mathrm{v}), \end{cases} \tag{4.4}$$

where

$$r_i(t) = \alpha_i - \beta_i \operatorname{sech}\left[\gamma\left(t - \frac{t_1 + t_2}{2}\right)\right], \tag{4.5a}$$

$$\Delta_i(t) = -\Omega \exp\left[-\left(\frac{t - t_i}{(1-\gamma)(t_1 - t_2)}\right)^2\right] + \Delta_i, \tag{4.5b}$$

and where r_v is the radius of the point of intersection of $V_{1,2}$. As initial state we choose the ground state of the potential V_1 at $t = 0$; for the parameters we use $\omega = 20.0, \Omega = 10, \Delta_1 = 0.0, t_1 = 15.0, t_2 = 10.0, \alpha_1 = 4.5, \alpha_2 = 7.5, \beta_1 = -\beta_2 = 1.0$, and $\gamma = 0.30$. The potential V causes a state transfer process, whereby the occupation moves from V_1 to V_2, during which a controlled number of RDSs will be printed, determined by the remaining parameter Δ_2 (see Fig. 4.2).

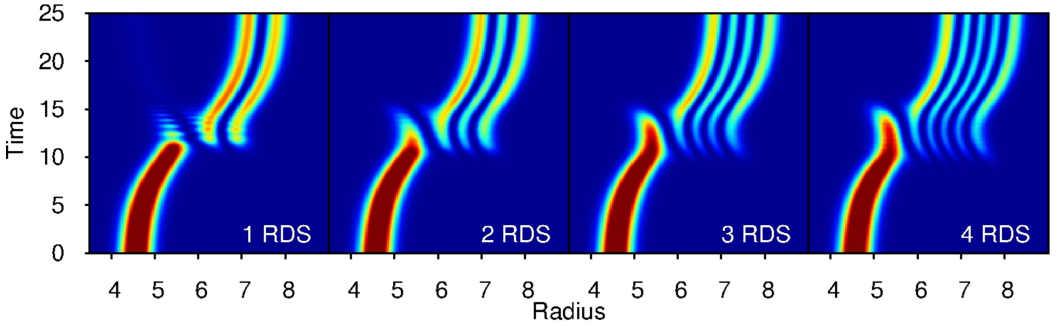

Figure 4.2: Density plots of the creation of multiple RDSs in a toroidal BEC using the potential (4.4). Here $C_{2\mathrm{D}} = 50$. The colouring is as in Fig. 4.1, but the density is normalised to unity. (1RDS) $\Delta_2 = -15.0$. (2RDS) $\Delta_2 = -35.0$. (3RDS) $\Delta_2 = -60.0$. (4RDS) $\Delta_2 = -80.0$.

The strict controllability sets this protocol aside from the one presented in Sec. 4.1, but it is more difficult to realise experimentally (however, the sharp cusp at $r = r_{\mathrm{v}}$ is not a physically relevant feature). Still, with modern advances in methods for painting arbitrary time-averaged potentials [124, 125], the potential (4.4) is feasible (see Publication III for details).

We model the observed dynamics in terms of inter-well tunnelling followed by self-interference of the condensate. In the rest of this section, we study the appearance of the self-interference fringes in terms of the Wigner function and the method of images.

Wigner Function

Matter-wave interference is quintessentially a quantum-mechanical phenomenon, and as such the self-interference of Sec. 4.2 is non-classical. The Wigner function representation [126] $W_\psi \in \mathbb{R}$ of the state $|\psi\rangle$,

$$W_\psi(\mathbf{r}, \mathbf{p}) = \frac{1}{(2\pi)^2} \int_{\mathbb{R}^2} \mathrm{d}\mathbf{u}\, \psi^* \left(\mathbf{r} - \frac{\mathbf{u}}{2}\right) \psi \left(\mathbf{r} + \frac{\mathbf{u}}{2}\right) \mathrm{e}^{-\mathrm{i}\mathbf{u}\cdot\mathbf{p}}, \tag{4.6}$$

with the marginals

$$\int_{\mathbb{R}^2} \mathrm{d}\mathbf{p}\, W_\psi(\mathbf{r}, \mathbf{p}) = |\, \langle \mathbf{r} \,|\, \psi \rangle \,|^2, \qquad \int_{\mathbb{R}^2} \mathrm{d}\mathbf{r}\, W_\psi(\mathbf{r}, \mathbf{p}) = |\, \langle \mathbf{p} \,|\, \psi \rangle \,|^2, \tag{4.7}$$

is often quite suitable for presenting non-classical states, and in Fig. 4.3 we have evaluated W_ψ corresponding to some of the states in Fig. 4.2 (see Sec. 3.1. of Publication IV for the same discussion related to Sec. 4.1). A necessary and sufficient condition for the Wigner function to be a true phase space density [127] states that this happens only for coherent and squeezed vacuum states (Gaussian states), and we associate the negativity of the Wigner function with the emergence of toroidal matter-wave interference.

Initially, the Wigner function is positive around $r = 4.5$, and fringes only appear in the (magnitude of the) momentum near $r = 0$ [see $t = 0.0$, Fig. 4.3 (a)]. The position distribution $|\psi(r)|^2 = 0$ vanishes in that region, but the Wigner function is reminiscent of that of the Schrödinger cat state, so the fringes seen here seem to be related to the opposite parts of the BEC ring interfering with each other (see Sec. 4.1). However, as the condensate is being propagated in the potential (4.4), the central fringes near the origin disappear, and we can see the appearance of fringes that give rise to oscillations in the position representation [see $t = 11.5$, Figs. 4.3 (b)-(c)]. This behaviour reflects the self-interference of the condensate in the outer potential. At the end of the well transfer process [see $t = 25.0$, Figs. 4.3 (d)-(e)], RDSs have appeared,

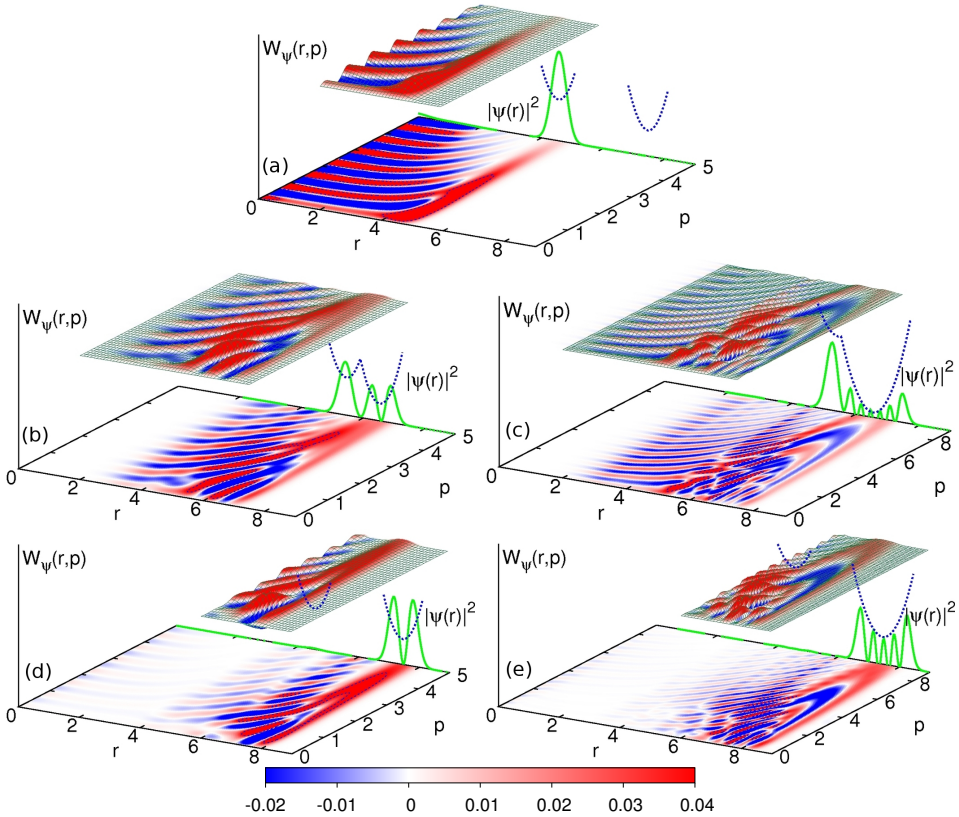

Figure 4.3: Time evolution of the Wigner function corresponding to the creation of a single (left, $\Delta_2 = -15$) and four (right, $\Delta_2 = -80$) RDS(s) in the potential V [blue dashed lines, see Eq. (4.4)]. For the 4RDS case here we use $\Omega = 35$, but the process is robust against (small) variations of parameters. The green solid line shows $|\psi(r)|^2$ evaluated as the marginal over p [see Eq. (4.7)]. (a) $t = 0.0$. (b)-(c) $t = 11.5$. (d)-(e) $t = 25.0$.

involving negative regions of the Wigner function. The dark soliton is not a classical state.

Method of Images

One way to model the dynamics in the toroidal double-well (4.4) is to invoke the method of images [128]. To this end, we approximate the potential by

$$V(r) = \begin{cases} V_1 & \text{if } r_1 < r \leq r_2 \\ V_2 & \text{if } r_2 < r \leq r_3 \\ \infty & \text{otherwise,} \end{cases} \tag{4.8}$$

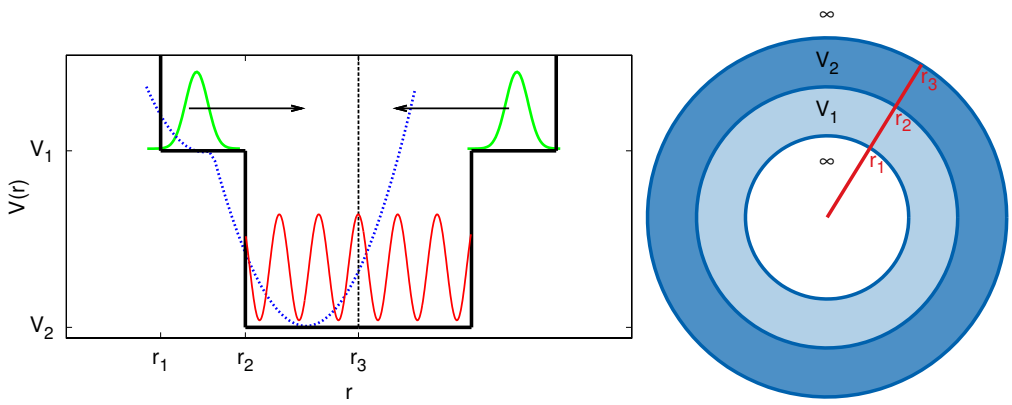

Figure 4.4: Left panel: Radial slice of the approximative step potential (4.8) (solid black line) ($r \leq r3$) and its image ($r > r_3$). The real double-well potential (4.4) at $t = 11.5$ for the production of four RDSs is also shown (dashed blue line). The initial position distribution $|\psi(r,0)|^2$ and its image are displayed (solid green line); their interference takes place in the lower well, which is shown schematically with the cosine wave (solid red line). The real wave function is zero at $r \geq r_3$. Right panel: The potential (4.8) on the full ring geometry.

where $V_{1,2}$ are constants such that $V_2 < V_1$ (see Fig. 4.4). Numerical simulations of the GPE (4.3) with the potential (4.8) show that the fringe separation is to a high degree determined by the relative depth $\Delta V = |V_2 - V_1|$ of the outer well. The larger the depth, the closer the fringes are separated. The width $L = r_3 - r_2$ of the outer well then determines how many fringes fit.

Ignoring interactions, let us consider the initial state and potential to be given by Eq. (4.2). As a further simplification, we assume that we have a one-dimensional planar system with no effects from the radial geometry, and that the transmission through the step results in another Gaussian wave packet. Reflection of the wave packet in the region $r \leq r_2$ is ignored as we are interested only in the transmitted part, whose broadening we also ignore for simplicity. Being lower in energy by ΔV, the outer well imparts[3] some net momentum k: $\psi(r,0) \to \tilde{\varphi}_{\mathrm{G}}(r,0) = \varphi_{\mathrm{G}}(r,0)\mathrm{e}^{\mathrm{i}kr}$.

The transmitted wave packet will then interfere with its image, producing the fringes. The de Broglie wavelength $\lambda = h/(mv)$, where v is the relative centre of mass speed between the (point-like) condensate and the image, gives a first measure of the fringe spacing; in our scalings[4], $\lambda = \pi/k$. Clearly, the

[3] Without loss of generality we can choose $V_1 = 0$, in which case the mean wavenumber $k = \sqrt{k_{\mathrm{i}}^2}$ at $r \leq r_2$ and $k = \sqrt{k_{\mathrm{i}}^2 - (-V_2)} = \sqrt{k_{\mathrm{i}}^2 + \Delta V}$ at $r > r_2$, where k_{i}^2 is the initial kinetic energy. In the text $\varphi_{\mathrm{G}}(r,0)$ corresponds to $k_{\mathrm{i}} = 0$ [see Eq. (4.2)].

[4] We have $v = 2v_{\mathrm{g}} = 4k$, where v_{g} is the group velocity of $\tilde{\varphi}_{\mathrm{G}}(r,t)$ [see Eq. (4.9)] and $m = 0.5, h = 2\pi$.

larger ΔV is, the larger the imparted momentum k becomes, and therefore the closer the fringes get. After solving the Schrödinger equation for free particles to get the time evolution of the wave packet, and assuming that the transmitted condensate in the outer well is located at $r_0 = r_3 - d/2$ at $t = 0$, we obtain

$$\tilde{\varphi}_{\mathrm{G}}(r,t) = \frac{\mathcal{N}}{\sqrt{1+\mathrm{i}\omega t}} \exp\left[-\frac{\sigma^2 k^2}{2} - \frac{(r - r_3 + d/2 - \mathrm{i}\sigma^2 k)^2}{2\sigma^2(1+\mathrm{i}\omega t)}\right]. \tag{4.9}$$

Equation (4.9) represents a Gaussian wave packet that travels at the group velocity $v_{\mathrm{g}} = 2k$ to the right.

To satisfy the zero boundary condition at $r = r_3$, we write the wave function as a sum of a Gaussian wave packet approaching from the left (smaller radius), $\tilde{\varphi}^{-}_{\mathrm{G}}(r,t)$ with $v_{\mathrm{g}} = 2k$, and its mirror image approaching from the right (larger radius), $\tilde{\varphi}^{+}_{\mathrm{G}}(r,t)$, which is only valid for $r \leq r_3$:

$$\psi(r,t) = \tilde{\varphi}^{-}_{\mathrm{G}}(r,t) - \tilde{\varphi}^{+}_{\mathrm{G}}(r,t), \tag{4.10}$$

where the $\tilde{\varphi}^{\pm}_{\mathrm{G}}(r,t)$ are located at $r_0 = r_3 \pm d/2$ at $t = 0$ respectively[5]. At $r \geq r_3$, $\psi = 0$. The interference term in $|\psi(r,t)|^2$, $I = \mathrm{Re}\{\tilde{\varphi}^{-}_{\mathrm{G}}(r,t)[\tilde{\varphi}^{+}_{\mathrm{G}}(r,t)]^*\}$, becomes

$$I \propto \cos\left[\frac{(r - r_3)(2k\sigma^2 + dt\omega)}{\sigma^2(1 + t^2\omega^2)}\right], \tag{4.11}$$

showing that a larger k leads to more closely separated fringes.

Since[6] $v = d/t = 2v_{\mathrm{g}}$, using the group velocity $v_{\mathrm{g}} = 2k$, we obtain $k = d/(4t)$, and therefore the fringe spacing in Eq. (4.11) becomes

$$\Delta r = \frac{4\pi}{v} = \frac{\pi}{k}. \tag{4.12}$$

In SI-units, $\Delta r = h/(mv)$, recovering the earlier de Broglie result. If the initial kinetic energy is k_{i}^2, we can write $k = \sqrt{k_{\mathrm{i}}^2 + \Delta V}$ (see Footnote 3) to obtain

$$\Delta r = \frac{\pi}{\sqrt{k_{\mathrm{i}}^2 + \Delta V}}, \tag{4.13}$$

showing how the relative depth ΔV of the outer well affects the fringe spacing Δr. The number of fringes is then kL/π. Despite its simplicity, the image model captures the essential physics in terms of showing that a deeper outer well results in more solitons (see Publication III).

[5] Explicitly, $\tilde{\varphi}^{\pm}_{\mathrm{G}}(r,t) \propto \exp\left[-\frac{(r - r_3 \mp \frac{d}{2} \pm \mathrm{i}\sigma^2 k)^2}{2\sigma^2(1+\mathrm{i}\omega t)}\right]$, and $\sigma^2 = 2/\omega$.

[6] We write $v = d/t$ in the same sense as in Ref. [110], i.e. t is the time between letting the condensate expand freely and making the observation.

Chapter 5

Decay of Ring Dark Solitons

The protocols for the creation of RDSs presented in Chapter 4 avoid the snake instability if a sufficiently low value of C_{2D} is used [see Eq. (4.3)]. On the other hand, when C_{2D} is ramped up, the snake instability occurs, which is responsible for the (generally thought irreversible) decay of the RDSs into vortex-antivortex pairs, or vortex rings in three dimensions. In Publications II and III, however, it was discovered that the snake instability can in fact be reversible, but eventually the condensate ends up manifesting quantum turbulence [129] (see Publication III for details). In Publication V, we study in detail using the method of images how and when the revival occurs.

It is well known that a lone vortex-antivortex pair, also known as a vortex dipole, can periodically annihilate itself to form a short dark (grey) soliton and appear again [130, 131]. Indeed, in a cigar-shaped condensate, periodic oscillations between a vortex-antivortex pair and a short dark soliton have been experimentally observed [115], but a RDS is at least an order of magnitude longer in length, correspondingly producing several vortex-antivortex pairs. Their remarkable recombination back to the RDS is unintuitive, and an example of coherent vortex dynamics before the onset of quantum turbulence.

In this Chapter, we first discuss the snake instability of RDSs (see Sec. 5.1), and then briefly outline when it is reversible or even suppressed making the RDS long-lived (see Sec. 5.2).

5.1 Snake Instability

In two dimensions, in general, the (ring) dark soliton notch starts undulating in a snake-like manner [42], until a (circular) array of vortex-antivortex pairs results [40, 58, 59, 132–134]. In three-dimensional systems, the snake instability results in vortex rings [65].

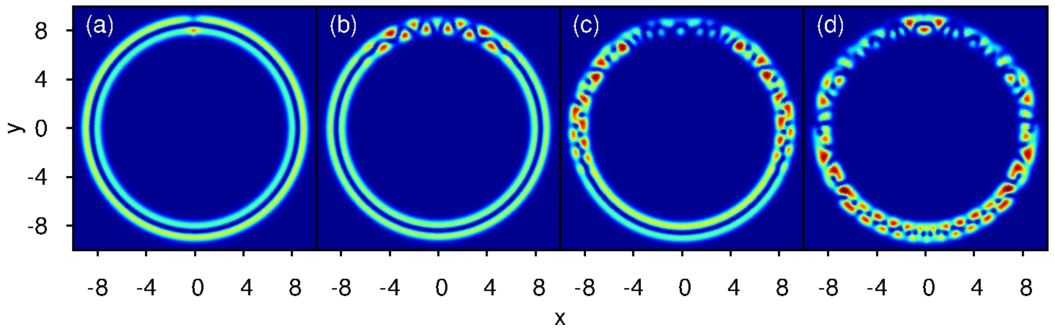

Figure 5.1: Density plots of the snake instability, after the cylindrical symmetry has been broken. The colouring is as in Fig. 4.1, but the density is normalised to unity. (a) $t = 0.0$. (b) $t = 1.5$. (c) $t = 3.0$. (d) $t = 4.4$.

In Publication II, we show that the snake instability follows only after a symmetry breaking; subsequently an unbalanced quantum pressure on opposite sides of the (ring) dark soliton notch starts generating the transverse perturbations. In Fig. 5.1, we numerically integrate the GPE (4.3) on a polar grid with $C_{2D} = 400$, $V = 24(r - 8.5)^2$, and artificially break the angular symmetry by having a small dent in the trapping potential [see Fig. 5.1(a)]. The particular shape of the anisotropy was not observed to matter. The snake instability ensues, producing multiple vortex-antivortex pairs.

The snake instability has been shown to be linked with complex frequencies in the Bogoliubov-de Gennes (BdG) (see Sec. 2.3) excitation spectrum [65, 135]. In Publication II, we further elucidate the role of the imaginary BdG modes in driving the instability, focussing on RDSs. The BdG equations (2.40) are a linear approximation, and the modes are valid for short enough time-scales. Eventually the linearisation will fail, and the imaginary instability modes result in a vortex-antivortex necklace.

5.2 RDS Revival as a Boundary Effect

The snake instability can be suppressed if the longitudinal length of the soliton notch is small enough [61, 136] (with respect to the instability wavenumber band). In Publication V, we show that a similar suppression occurs even with a long RDS, provided that in this case the transverse confinement is tight enough (see Ref. [137] for a similar result). In particular, we require $d \lesssim 3\xi$, where d is the radial width of a toroidal condensate containing the RDS. In addition, we show that the original RDS is revived from the vortex-antivortex necklace when $d \lesssim 16\xi$.

Chapter 6

Conclusion

In this Thesis, we have studied the creation and dynamics of ring dark solitons in toroidally trapped quasi-two-dimensional Bose-Einstein condensates. We refer the reader to the concluding sections in the Publications (see Page iv); their main results are listed below:

Publication I: Exact soliton-like ring solutions of the cylindrically symmetric Gross-Pitaevskii equation were found. In addition, we found exact solutions that describe scattering (one-time or periodic) from the central potential of a bright ring.

Publication II: We showed that a symmetry breaking is a necessary requirement for the snake instability of a (ring) dark soliton. We explained the snake instability in terms of an unbalanced quantum pressure across the soliton's notch, and showed explicitly how the snake instability of a ring dark soliton appears in the Bogoliubov-de Gennes spectrum.

Publication III: We proposed an experimentally feasible protocol for the controlled creation of multiple concentric ring dark solitons in a ring-shaped condensate. We showed that the snake instability can be reversible even in the case of a many-RDS system, but eventually it leads to an example of quantum turbulence.

Publication IV: We showed analytically how the free expansion of a ring-shaped condensate results in self-interference with the fringes given by a Bessel function modulation, which can be used to create ring dark solitons as well. In particular, we showed that an initial persistent current in the ring makes the self-interference impossible in the free expansion, but instead results in a long-lived density hole at the centre.

Publication V: We showed theoretically that the reversibility of the snake instability of a ring dark soliton results from boundary effects. If the condensate boundary is restrictive enough, the ring dark soliton becomes long-lived.

We have focussed on atomic Bose-Einstein condensates, but the Gross-Pitaevskii equation is more universal with analogous systems in nonlinear optics and exciton-polariton microcavities [96], for example. Indeed, in Sec. 3.2 we saw how the exact soliton-like dark ring solution (3.23) has been encountered in an experiment regarding a polariton condensate. Still, our results open new directions for atomic condensates as well by firstly demonstrating how to experimentally create ring dark solitons.

Secondly, the results of this Thesis for the subsequent behaviour of the ring dark soliton(s), in particular the possible reversibility of the snake instability, present an example of coherent vortex dynamics before the onset of quantum turbulence. Despite the lack of known exact ring dark soliton solutions of the Gross-Pitaevskii equation, our results show that at least exact soliton-like solutions do exist, and that ring dark solitons can in fact have rich dynamics in toroidal traps.

Moreover, the stabilisation of a (ring) dark soliton under tight transverse trapping poses interesting questions. Can we build a matter-wave switch, i.e. let the dark soliton notch act as a waveguide for a weak signal changing its direction or location? Is it possible to take this idea even further by considering a wire, an extension to the matter-wave side of the concept of an optical fibre, made out of a long and narrow condensate that has a dark soliton in the longitudinal direction?

References

[1] J. E. Oliver, *The Encyclopedia of World Climatology* (Springer, 2005).

[2] E. Joos, H. Zeh, C. Kiefer, D. Giulini, J. Kupsch, and I.-O. Stamatescu, *Decoherence and the Appearance of a Classical World in Quantum Theory*, 2nd ed. (Springer, 2003).

[3] S. Stenholm, Rev. Mod. Phys. **58**, 699 (1986).

[4] E. A. Cornell and C. E. Wieman, Rev. Mod. Phys. **74**, 875 (2002).

[5] W. Ketterle, Rev. Mod. Phys. **74**, 1131 (2002).

[6] M. H. Anderson, J. R. Ensher, M. R. Matthews, C. E. Wieman, and E. A. Cornell, Science **269**, 198 (1995).

[7] K. B. Davis, M. O. Mewes, M. R. Andrews, N. J. van Druten, D. S. Durfee, D. M. Kurn, and W. Ketterle, Phys. Rev. Lett. **75**, 3969 (1995).

[8] C. Pethick and H. Smith, *Bose-Einstein Condensation in Dilute Gases*, 2nd ed. (Cambridge University Press, 2008).

[9] D. J. Fixsen, ApJ **707**, 916 (2009).

[10] S. N. Bose, Z. Phys. **26**, 178 (1924).

[11] A. Einstein, Sitzber. Kgl. Preuss. Akad. Wiss. **261** (1924).

[12] P. L. Kapitza, Nature **141**, 74 (1938).

[13] J. F. Allen and A. D. Misener, Nature **141**, 75 (1938).

[14] F. London, Nature **141**, 643 (1938).

[15] O. Penrose and L. Onsager, Phys. Rev. **104**, 576 (1956).

[16] H. R. Glyde, Phys. Rev. B **50**, 6726 (1994).

[17] H. R. Glyde, R. T. Azuah, and W. G. Stirling, Phys. Rev. B **62**, 14337 (2000).

[18] S. Moroni, G. Senatore, and S. Fantoni, Phys. Rev. B **55**, 1040 (1997).

[19] A. Leggett, *Quantum Liquids* (Oxford University Press, 2006).

[20] N. D. Mermin and H. Wagner, Phys. Rev. Lett. **17**, 1133 (1966).

[21] P. C. Hohenberg, Phys. Rev. **158**, 383 (1967).

[22] J. M. Kosterlitz and D. J. Thouless, J. Phys. C **6**, 1181 (1973).

[23] V. L. Berezinskii, Sov. Phys. JETP **34**, 610 (1972).

[24] N. N. Bogoliubov, J. Phys. (USSR) **11**, 23 (1947).

[25] A. J. Leggett, New J. Phys. **5**, 103 (2003).

[26] H. J. Metcalf and P. van der Straten, *Laser Cooling and Trapping* (Springer, 1999).

[27] C. Chin, R. Grimm, P. Julienne, and E. Tiesinga, Rev. Mod. Phys. **82**, 1225 (2010).

[28] A. Görlitz, J. M. Vogels, A. E. Leanhardt, C. Raman, T. L. Gustavson, J. R. Abo-Shaeer, A. P. Chikkatur, S. Gupta, S. Inouye, T. Rosenband, and W. Ketterle, Phys. Rev. Lett. **87**, 130402 (2001).

[29] R. Dum, A. Sanpera, K.-A. Suominen, M. Brewczyk, M. Kuś, K. Rzążewski, and M. Lewenstein, Phys. Rev. Lett. **80**, 3899 (1998).

[30] T. Kuga, Y. Torii, N. Shiokawa, T. Hirano, Y. Shimizu, and H. Sasada, Phys. Rev. Lett. **78**, 4713 (1997).

[31] P. F. Griffin, E. Riis, and A. S. Arnold, Phys. Rev. A **77**, 051402 (2008).
[32] P. M. Baker, J. A. Stickney, M. B. Squires, J. A. Scoville, E. J. Carlson, W. R. Buchwald, and S. M. Miller, Phys. Rev. A **80**, 063615 (2009).
[33] B. E. Sherlock, M. Gildemeister, E. Owen, E. Nugent, and C. J. Foot, Phys. Rev. A **83**, 043408 (2011).
[34] O. Morizot, Y. Colombe, V. Lorent, H. Perrin, and B. M. Garraway, Phys. Rev. A **74**, 023617 (2006).
[35] I. Lesanovsky and W. von Klitzing, Phys. Rev. Lett. **99**, 083001 (2007).
[36] E. M. Wright, J. Arlt, and K. Dholakia, Phys. Rev. A **63**, 013608 (2000).
[37] W. H. Heathcote, E. Nugent, B. T. Sheard, and C. J. Foot, New J. Phys. **10**, 043012 (2008).
[38] E. P. Gross, Nuovo Cimento **20**, 454 (1961).
[39] L. P. Pitaevskii, Sov. Phys. JETP **13**, 451 (1961).
[40] Y. S. Kivshar and B. Luther-Davies, Phys. Rep. **298**, 81 (1998).
[41] P. G. Kevrekidis, D. J. Frantzeskakis, and R. Carretero-González (Eds.), *Emergent Nonlinear Phenomena in Bose-Einstein Condensates* (Springer, 2008).
[42] D. J. Frantzeskakis, J. Phys. A: Math. Theor. **43**, 213001 (2010).
[43] P. G. Drazin and R. S. Johnson, *Solitons: An Introduction*, 2nd ed. (Cambridge University Press, 1989).
[44] A. S. Davydov, *Solitons in Molecular Systems* (Springer, 1990).
[45] S. P. Novikov, S. V. Manakov, L. P. Pitaevskii, and V. E. Zakharov, *Theory of Solitons: Inverse Scattering Method* (Consultants Bureau, 1980).
[46] R. Hirota, *The Direct Method in Soliton Theory* (Cambridge University Press, 2004).
[47] A. Kundu, *Classical and Quantum Nonlinear Integrable Systems: Theory and Application* (Taylor & Francis, 2010).
[48] M. Jimbo, T. Miwa, and E. Date, *Solitons: Differential Equations, Symmetries and Infinite Dimensional Algebras* (Cambridge University Press, 2000).
[49] M. Antezza, F. Dalfovo, L. P. Pitaevskii, and S. Stringari, Phys. Rev. A **76**, 043610 (2007).
[50] R. G. Scott, F. Dalfovo, L. P. Pitaevskii, and S. Stringari, Phys. Rev. Lett. **106**, 185301 (2011).
[51] A. Spuntarelli, L. D. Carr, P. Pieri, and G. C. Strinati, New J. Phys. **13**, 035010 (2011).
[52] R. Liao and J. Brand, Phys. Rev. A **83**, 041604 (2011).
[53] N. S. Manton and P. Sutcliffe, *Topological Solitons* (Cambridge University Press, 2007).
[54] D. Tong, *TASI Lectures on Solitons*, arXiv:hep-th/0509216.
[55] T. Vachaspati, *Kinks and Domain Walls* (Cambridge University Press, 2006).
[56] G. A. Swartzlander and C. T. Law, Phys. Rev. Lett. **69**, 2503 (1992).
[57] S. Burger, K. Bongs, S. Dettmer, W. Ertmer, K. Sengstock, A. Sanpera, G. V. Shlyapnikov, and M. Lewenstein, Phys. Rev. Lett. **83**, 5198 (1999).

[58] Z. Dutton, M. Budde, C. Slowe, and L. V. Hau, Science **293**, 663 (2001).
[59] B. P. Anderson, P. C. Haljan, C. A. Regal, D. L. Feder, L. A. Collins, C. W. Clark, and E. A. Cornell, Phys. Rev. Lett. **86**, 2926 (2001).
[60] V. A. Brazhnyi and V. V. Konotop, Phys. Rev. A **68**, 043613 (2003).
[61] A. E. Muryshev, H. B. van Linden van den Heuvell, and G. V. Shlyapnikov, Phys. Rev. A **60**, R2665 (1999).
[62] Y. S. Kivshar and X. Yang, Phys. Rev. E **49**, 1657 (1994).
[63] G. Theocharis, P. Schmelcher, M. K. Oberthaler, P. G. Kevrekidis, and D. J. Frantzeskakis, Phys. Rev. A **72**, 023609 (2005).
[64] Y. S. Kivshar and X. Yang, Chaos, Solitons, and Fractals **4**, 1745 (1994).
[65] D. L. Feder, M. S. Pindzola, L. A. Collins, B. I. Schneider, and C. W. Clark, Phys. Rev. A **62**, 053606 (2000).
[66] L. D. Carr and C. W. Clark, Phys. Rev. Lett. **97**, 010403 (2006).
[67] Y. S. Kivshar and X. Yang, Phys. Rev. E **50**, R40 (1994).
[68] G. Theocharis, D. J. Frantzeskakis, P. G. Kevrekidis, B. A. Malomed, and Y. S. Kivshar, Phys. Rev. Lett. **90**, 120403 (2003).
[69] A. Dreischuh, D. Neshev, G. G. Paulus, F. Grasbon, and H. Walther, Phys. Rev. E **66**, 066611 (2002).
[70] G. Herring, L. D. Carr, R. Carretero-González, P. G. Kevrekidis, and D. J. Frantzeskakis, Phys. Rev. A **77**, 023625 (2008).
[71] I. Bloch, J. Dalibard, and W. Zwerger, Rev. Mod. Phys. **80**, 885 (2008).
[72] M. Lewenstein, A. Sanpera, and V. Ahufinger, *Ultracold Atoms in Optical Lattices* (Oxford University Press, 2012).
[73] J. Dalibard, F. Gerbier, G. Juzeliūnas, and P. Öhberg, Rev. Mod. Phys. **83**, 1523 (2011).
[74] G. E. Volovik, *The Universe in a Helium Droplet* (Oxford University Press, 2003).
[75] J. Klaers, J. Schmitt, F. Vewinger, and M. Weitz, Nature **468**, 545 (2010).
[76] C. N. Yang, Rev. Mod. Phys. **34**, 694 (1962).
[77] L. Pitaevskii and S. Stringari, *Bose-Einstein Condensation* (Oxford University Press, 2003).
[78] A. Altland and B. Simons, *Condensed Matter Field Theory* (Cambridge University Press, 2007).
[79] X.-G. Wen, *Quantum Field Theory of Many-body Systems* (Oxford University Press, 2004).
[80] A. J. Leggett, Rev. Mod. Phys. **73**, 307 (2001).
[81] A. L. Fetter, Rev. Mod. Phys. **81**, 647 (2009).
[82] M. Peskin and D. Schroeder, *An Introduction to Quantum Field Theory* (Addison-Wesley, 1995).
[83] D. M. Ceperley, Rev. Mod. Phys. **67**, 279 (1995).
[84] S. Geltman, EPL **87**, 13001 (2009).
[85] F. Dalfovo, S. Giorgini, L. P. Pitaevskii, and S. Stringari, Rev. Mod. Phys. **71**, 463 (1999).

[86] K. W. Madison, F. Chevy, W. Wohlleben, and J. Dalibard, Phys. Rev. Lett. **84**, 806 (2000).
[87] B. Alberts, A. Johnson, J. Lewis, M. Raff, K. Roberts, and P. Walter, *Molecular Biology of the Cell*, 5th ed. (Garland Science, 2008).
[88] N. D. Mermin and T.-L. Ho, Phys. Rev. Lett. **36**, 594 (1976).
[89] T. Mizushima, K. Machida, and T. Kita, Phys. Rev. Lett. **89**, 030401 (2002).
[90] L. M. Pismen, *Vortices in Nonlinear Fields* (Oxford University Press, 1999).
[91] P. O. Fedichev and G. V. Shlyapnikov, Phys. Rev. A **60**, R1779 (1999).
[92] V. E. Zakharov and A. B. Shabat, Sov. Phys. JETP **34**, 62 (1972).
[93] V. E. Zakharov and A. B. Shabat, Sov. Phys. JETP **37**, 823 (1973).
[94] T. Tsuzuki, J. Low Temp. Phys. **4**, 441 (1971).
[95] A. A. Svidzinsky and A. L. Fetter, Phys. Rev. A **58**, 3168 (1998).
[96] A. Bramati and M. Modugno (Eds.), *Physics of Quantum Fluids* (Springer, 2013).
[97] D. Zhao, X.-G. He, and H.-G. Luo, EPJ D **53**, 213 (2009).
[98] X.-G. He, D. Zhao, L. Li, and H.-G. Luo, Phys. Rev. E **79**, 056610 (2009).
[99] L. Gagnon and P. Winternitz, J. Phys. A: Math. Theor. **26**, 7061 (1993).
[100] J. Belmonte-Beitia, V. M. Pérez-García, V. Vekslerchik, and P. J. Torres, Phys. Rev. Lett. **98**, 064102 (2007).
[101] G. Bluman and J. Cole, *Similarity Methods for Differential Equations* (Springer, 1974).
[102] L. Dominici, D. Ballarini, M. De Giorgi, E. Cancellieri, B. Silva Fernández, A. Bramati, G. Gigli, F. Laussy, and D. Sanvitto, arXiv:1309.3083.
[103] S. A. Moskalenko and D. W. Snoke, *Bose-Einstein Condensation of Excitons and Biexcitons* (Cambridge University Press, 2005).
[104] A. Dreischuh, W. Fließer, I. Velchev, S. Dinev, and L. Windholz, Appl. Phys. B **62**, 139 (1996).
[105] H. E. Nistazakis, D. J. Frantzeskakis, B. A. Malomed, and P. G. Kevrekidis, Phys. Lett. A **285**, 157 (2001).
[106] L. D. Carr and C. W. Clark, Phys. Rev. A **74**, 043613 (2006).
[107] J. Denschlag, J. E. Simsarian, D. L. Feder, C. W. Clark, L. A. Collins, J. Cubizolles, L. Deng, E. W. Hagley, K. Helmerson, W. P. Reinhardt, S. L. Rolston, B. I. Schneider, and W. D. Phillips, Science **287**, 97 (2000).
[108] C. Becker, S. Stellmer, P. Soltan-Panahi, S. Dörscher, M. Baumert, E.-M. Richter, J. Kronjäger, K. Bongs, and K. Sengstock, Nature Physics **4**, 496 (2008).
[109] D. Neshev, A. Dreischuh, V. Kamenov, I. Stefanov, S. Dinev, W. Fließer, and L. Windholz, Appl. Phys. B **64**, 429 (1997).
[110] M. R. Andrews, C. G. Townsend, H.-J. Miesner, D. S. Durfee, D. M. Kurn, and W. Ketterle, Science **275**, 637 (1997).
[111] T. F. Scott, R. J. Ballagh, and K. Burnett, J. Phys. B: At. Mol. Opt. Phys. **31**, L329 (1998).
[112] A. Weller, J. P. Ronzheimer, C. Gross, J. Esteve, M. K. Oberthaler, D. J.

Frantzeskakis, G. Theocharis, and P. G. Kevrekidis, Phys. Rev. Lett. **101**, 130401 (2008).
[113] G.-B. Jo, J.-H. Choi, C. A. Christensen, T. A. Pasquini, Y.-R. Lee, W. Ketterle, and D. E. Pritchard, Phys. Rev. Lett. **98**, 180401 (2007).
[114] W. P. Reinhardt and C. W. Clark, J. Phys. B: At. Mol. Opt. Phys. **30**, L785 (1997).
[115] I. Shomroni, E. Lahoud, S. Levy, and J. Steinhauer, Nature Physics **5**, 193 (2009).
[116] J. Ruostekoski, B. Kneer, W. P. Schleich, and G. Rempe, Phys. Rev. A **63**, 043613 (2001).
[117] S.-J. Yang, Q.-S. Wu, S.-N. Zhang, S. Feng, W. Guo, Y.-C. Wen, and Y. Yu, Phys. Rev. A **76**, 063606 (2007).
[118] B. M. Garraway and K.-A. Suominen, Phys. Rev. Lett. **80**, 932 (1998).
[119] K. Härkönen, O. Kärki, and K.-A. Suominen, Phys. Rev. A **74**, 043404 (2006).
[120] Y. S. Kivshar, T. J. Alexander, and S. K. Turitsyn, Phys. Lett. A **278**, 225 (2001).
[121] C. Lee, E. A. Ostrovskaya, and Y. S. Kivshar, J. Phys. B: At. Mol. Opt. Phys. **40**, 4235 (2007).
[122] C. Ryu, K. C. Henderson, and M. G. Boshier, New J. Phys. **16**, 013046 (2014).
[123] M. Abramowitz and I. A. Stegun, *Handbook of Mathematical Functions* (Dover, 1964).
[124] K. Henderson, C. Ryu, C. MacCormick, and M. G. Boshier, New J. Phys. **11**, 043030 (2009).
[125] C. Ryu, P. W. Blackburn, A. A. Blinova, and M. G. Boshier, Phys. Rev. Lett. **111**, 205301 (2013).
[126] E. Wigner, Phys. Rev. **40**, 749 (1932).
[127] R. L. Hudson, Rep. Math. Phys. **6**, 249 (1974).
[128] R. W. Robinett, Physica Scripta **73**, 681 (2006).
[129] U. Frisch and A. Kolmogorov, *Turbulence* (Cambridge University Press, 1995).
[130] A. Klein, D. Jaksch, Y. Zhang, and W. Bao, Phys. Rev. A **76**, 043602 (2007).
[131] L.-C. Crasovan, V. Vekslerchik, V. M. Pérez-García, J. P. Torres, D. Mihalache, and L. Torner, Phys. Rev. A **68**, 063609 (2003).
[132] A. V. Mamaev, M. Saffman, and A. A. Zozulya, Phys. Rev. Lett. **76**, 2262 (1996).
[133] Y. S. Kivshar and D. E. Pelinovsky, Phys. Rep. **331**, 117 (2000).
[134] V. Tikhonenko, J. Christou, B. Luther-Davies, and Y. S. Kivshar, Opt. Lett. **21**, 1129 (1996).
[135] T. Morgan and T. Busch, Phys. Rev. A **88**, 063610 (2013).
[136] P. G. Kevrekidis, G. Theocharis, D. J. Frantzeskakis, and A. Trombettoni, Phys. Rev. A **70**, 023602 (2004).
[137] M. Ma, R. Carretero-González, P. G. Kevrekidis, D. J. Frantzeskakis, and B. A. Malomed, Phys. Rev. A **82**, 023621 (2010).